TÉCNICO LISBOA

Sizing of the Electric Traction System for a Solar Competition Vehicle

Guilherme Silva Carvalho

Thesis to obtain the Master of Science Degree in

Electrical and Computer Engineering

Supervisors: Prof. Paulo José da Costa Branco
Prof. João Paulo Neto Torres

Examination Committee

Chairperson: Prof. Célia Maria Santos Cardoso de Jesus
Supervisor: Prof. Paulo José da Costa Branco
Member of the Committee: Prof. João Filipe Pereira Fernandes

7 November 2024

Declaration

I declare that this document is an original work of my own authorship and that it fulfills all the requirements of the Code of Conduct and Good Practices of the Universidade de Lisboa.

Acknowledgments

I would like to express my gratitude to everyone who helped me throughout the completion of my master's degree. It is thanks to these people that I was able to finish this project. I thank everyone, my family, colleagues, friends, and professors who supported me. I want to especially thank my parents and my brother for their support and effort throughout this journey. To my girlfriend, who has always supported me. To Ricardo Lameirinhas and Catarina Bernardo, for all their time, support, and effort throughout this project. Finally, to Professor Paulo Branco, for his guidance, time, and friendship provided. Please know that, no matter how small the help was, it did not go unnoticed. For this reason, I thank everyone who helped me and with whom I shared great moments during my master's.

Thank you all for your support!

Abstract

The objective of this project is to develop a tool that will facilitate the future design of a photovoltaic-powered vehicle for the Mobile Energy Sustainability Project (PSEM) team, enabling their participation in a solar competition.

To achieve this objective, a comparative analysis is conducted between various solar competitions, including the one currently attended by the team. The environmental conditions of these solar competitions are subjected to analysis. Subsequently, the analysis is directed to the World Solar Challenge, a solar competition that covers 3,000 km, comprising 10 segments extending from north to south Australia. The previously mentioned tool is utilized to simulate the vehicle's performance as it crosses the competition segments, using data from the event held in October 2019. As a result, the battery state of charge and the time required for the vehicle to complete each segment can be determined.

It can be concluded that the selected competition offers advantageous conditions for the vehicles. However, it is important to maximize energy production and optimize the vehicle as much as possible to reduce its consumption. In this regard, it is evident that aerodynamic resistance contributes most significantly to energy usage. In the future, it would be beneficial to conduct studies on the vehicle's components, such as battery degradation over time and increasing the photovoltaic surface area on the vehicle. Furthermore, it would be valuable to incorporate variable efficiencies for the motor and battery during the simulations.

Keywords

Solar car; Solar Competitions; Solar vehicle; Vehicle's powered by photovoltaic energy; World Solar Challenge.

Resumo

Este projeto pretende desenvolver uma ferramenta que permita ajudar na futura projeção de um veículo movido a energia fotovoltaica com a equipa do Projeto de Sustentabilidade Energética Móvel (PSEM) para participar numa competição solar.

Para tal, estudam-se várias competições solares e a competição atualmente frequentada pela equipa, identificando as diferenças entre as mesmas. Analisam-se as condições ambientais para as várias competições solares. Decide-se concentrar a análise na competição solar, World Solar Challenge, onde se percorrem 3000 km divididos por 10 segmentos de norte a sul da Austrália. Utilizando a ferramenta mencionada para realizar simulações do veículo a percorrer os vários segmentos da competição, utilizando dados da competição que ocorreu em outubro de 2019. Obtendo-se assim, o estado de carga da bateria e o tempo necessário para o veículo percorrer cada segmento.

Conclui-se, que a competição escolhida apresenta boas condições para os veículos, porém, é necessário maximizar a produção de energia e otimizar ao máximo o veículo de modo a reduzir o consumo, em que a resistência aerodinâmica apresenta o maior peso do consumo. Futuramente, seria benéfico realizar estudos para os componentes usados no veículo, como a degradação das baterias com a sua utilização e o aumento da área fotovoltaica instalada no veículo e também incluir eficiências variáveis para o motor e para a bateria durante as simulações.

Palavras Chave

Carro solar; Competições solares; Veículos movidos a energia fotovoltaica; Veículos solares; World Solar Challenge.

Contents

List of Figures

List of Tables

Symbology

g Acceleration of gravity, 9.81 m/s^2

C_d Aerodynamic drag coefficient

F_d Aerodynamic drag force

P_d Aerodynamic drag power

T_{amb} Ambient temperature

θ Angle between the car and the wind

T_{cell} Cell temperature

Crr Coefficient of rolling resistance

Z_w Distance of the ground for v_w in meters

Z_{w10m} Distance of the ground for $v_w 10m$ in meters

η_{cell} Efficiency of the cells

M_{eq} Equivalent total mass of the vehicle

F_{roll} Frictional force between the ground and the wheel

P_{roll} Frictional power between the ground and the wheel

F_g' Gravitational force component

P_g' Gravitational power component

I_w Inertia of rotational parts the vehicle

P_{Cin} Input power of the photovoltaic cells

G Irradiance

f_m	Mass factor
P_{Cout}	Output power of the photovoltaic cells
P_p	Peak power of the photovoltaic cells
ρ_{air}	Relative air density at 15 ℃
φ	Road inclination
T^r	Standard test condition cell temperature, 25 [ºC]
G^r	Standard test condition irradiance, 1000 [W/m^2]
μ_{pp}	Temperature coefficient
F_t	Traction force
P_t	Traction power
T_t	Traction torque
a	Vehicle acceleration
A_f	Vehicle frontal area
M	Vehicle plus driver mass
v_c	Vehicle speed
r_w	Wheel radius
α_w	Wheel rotational acceleration
ω_w	Wheel rotational speed
T_w	Wheel torque
v_w	Wind speed at 0.5 meter of the ground
v_{w10m}	Wind speed at 10 meter of the ground

Acronyms

ASC American Solar Challenge

CSA Carrera Solar Atacama

iESC iLumen European Solar Challenge

ISC Italian Solar Challenge

NOCT Nominal Operation Cell Temperature

PSEM Mobile Energy Sustainability Project (Projeto Sustentabilidade Energética Móvel)

SSC Sasol Solar Challenge

SCM Solar Challenge Morocco

WSC World Solar Challenge

1

Introduction

Contents

1.1 Motivation

The objective of this project is to develop a tool to support the future design of an electric traction system for a photovoltaic-powered vehicle.In recent years, there has been a notable surge in adopting more efficient and sustainable solutions within the transportation sector. Vehicle companies are allocating resources towards the energy transition, with a primary objective of reducing CO_2 emissions and pursuing environmentally-friendly alternatives for the future of vehicles. The European Commission has already taken a definitive stance, stating that ”all new cars and vans registered in Europe will be electric with zero-emissions by 2035” [2].

One of the major disadvantages of electric vehicles is the wait time to charge their batteries, which is especially problematic during long trips. The implementation of solar photovoltaic technology has the potential to extend the autonomy of electric vehicles, thereby representing an opportunity to develop a more sustainable mobile solution. This is because it involves the application of a renewable energy source, which contributes to the progression of transportation vehicles towards a more sustainable future.

1.2 Objectives

The main objective at this thesis is to assist the team Mobile Energy Sustainability Project (Projeto Sustentabilidade Energética Móvel) (PSEM) to a future size of an electric vehicle to participate in the Bridgestone World Solar Challenge, with photovoltaic cells as the main energy source of the vehicle.

To reach the main objective, the following methodology is needed:

Conduct an analysis of the environmental conditions at the locations where the competitions occur, assessing the specific conditions in each region for each competition;

Compare the competition that the team currently participates in with the new solar competitions;

Develop a tool that simulates the vehicle crossing the competition, thereby facilitating the acquisition of essential parameters for the vehicle's future sizing.

1.3 Outline

The project is structured into five parts. The first chapter introduces the motivation behind the project choice and outlines its objectives. The second chapter, entitled 'Solar Car Competitions', contains a comparison of the various competitions. The third chapter outlines the methodology employed for the project development. The fourth chapter includes the results obtained and their analysis, following the methodology discussed in the previous chapter. The fifth and final chapter is the conclusion, in which the achieved objectives are summarised and aspects of the project for improvement are referenced.

2

Solar Car Competitions

Contents

2.1 Introdution

In this chapter, a brief overview is provided about the Greenpower F24+ competition, which is currently attended by the PSEM team. It outlines the teams that made it to the podium in the competition and explains how the competition scoring is conducted. The chapter details the type of vehicles used, similar to those of the PSEM team. It references the solar competitions under study, identifying the teams that won the recent competitions and the latest vehicles from teams that consistently reached the podium. Some characteristics of these vehicles are highlighted. A comparison is drawn between the track types of these competitions and the Greenpower F24+, highlighting potential challenges that can be expected.

2.2 Greenpower Formula 24+

The PSEM team is actively engaged in the Greenpower F24+ competition, which allows teams to construct a vehicle. Teams may select either the option of purchasing a kit for vehicle construction or the alternative of constructing the vehicle from scratch. The F24+ events are conducted on closed circuits, with teams striving to complete the maximum number of laps within 60 minutes, though this may vary. In the F24+ category, the minimum age for team drivers is 16, with a maximum age of 25. Additionally, there is no limit on the number of drivers per team, requiring at least one driver per team. The potential issue of underage drivers may be the rationale behind using a closed circuit at the race track.

In the 2023 season of this competition, the scoring system utilized the following methodology: A total of 11 races were conducted between April and October, followed by a final race. During the initial phase, which consisted of the eleven races, teams were permitted to participate in order to earn as many points as possible. The team that finished in first place in any of these races was awarded 25 points. It was not mandatory for teams to participate in all eleven races and only the two best results achieved by each team during this phase were taken into consideration, achieving a maximum of 50 point. The total of these results is displayed in the ”Sub-Total” column of Table (2.1). This permitted teams to participate in multiple races with the objective of obtaining the 50 points during this phase. Subsequently, the final race was held, in which the team that finished first was awarded 25 points, as illustrated in the ”Final” column of Table (2.1). Ultimately, the ”Total” column indicates the overall score achieved by each team, which is the sum of the ”Sub-Total” and ”Final” columns, determining the winning team. Additionally, the table also includes links to the cars that participated in the 2023 season, except for the second and third-place teams, where the link directs to the sponsors of the respective teams, as the team pages with the cars could not be located.

Table 2.1: Top 4 teams for Greenpower Formula 24+ in 2023 from [1].

Pos	Car	Team	Entrant	Sub-Total	Final	Total
1	772	GP23 [3]	Instituto Superior Técnico	50	25	75
2	702	RENovation [4]	Renishaw plc	50	15	65
3	706	Probation IV [4]	Renishaw plc	50	8	58
4	703	Hades [5]	Coalescence	36	18	54

2.3 Solar Car Competitions and its Vehicles

There are several solar competitions worldwide. The ones chosen to study are selected based on their prestige and from different locations around the globe, addressing various environmental conditions. This allows us to observe the vehicle's behavior when exposed to different conditions. The selected competitions are American Solar Challenge (ASC) in the United States of America, World Solar Challenge (WSC) in Australia, Italian Solar Challenge (ISC) in Italy, iLumen European Solar Challenge (iESC) in Belgium, Sasol Solar Challenge (SSC) in South Africa, Carrera Solar Atacama (CSA) in Chile and Solar Challenge Morocco (SCM) in Morocco.

These competitions aim to build a vehicle powered by photovoltaic solar energy. Of the presented competitions, most have the same vehicle classes, with slight variations in details and class names, but the underlying principle remains the same. The ISC, SCM and CSA competitions have only two classes. The classes are divided into single-vehicle occupants, a vehicle for more than one person as in [6], and the last one for vehicles that do not qualify for any previous classes and exist for some of the solar competitions. Among these three classes, the most similar to the Greenpower F24+ is the single-occupant vehicle, intending to complete the route in the shortest possible time for the endurance events and the maximum number of laps in a given time for the track events. Below, the teams that reached the top 3 in each competition will be presented.

Based on the results of the recent competitions, the Table (2.2) shows the top 3 teams of each competition. One can see that for the iESC, the German team got the two first positions, this is because it it possible for the teams to participate with 2 cars. The teams colored are the ones that have more than one position in the different competitions. Agoria team changed the name to Innoptus, which is why they have the same color. It is observed that the teams Innoptus, Twente, and Brunel are the ones with the best results in road competitions, while in track competitions such as iESC and ISC, the Sonnewagen Aachen team achieves better results. The links on the right side of each competition are the websites that contain the top 3 results. The links located to the right of the color-highlighted teams grant access to the respective vehicles. These may not correspond to those used in the specific competition, but they represent the latest and currently available models for viewing. A notable common feature among these teams' vehicles is the incorporation of a flat surface area, with the objective of optimizing the utilization of photovoltaic cells. The majority of the vehicles have a 'bullet' shape, extending the placement of solar cells behind the driver. This design strategy maximizes the irradiance captured by the cells and allows the vehicle to have a low aerodynamic resistance. However, the Brunel Solar team's vehicle diverges from this trend, featuring the driver on one side, a third wheel on the opposite side, and the solar cells positioned in between, with the thinnest possible thickness. Unlike the Greenpower F24+, which features vehicles with a similar shape, solar competitions exhibit more diversity in vehicle construction, providing teams with fewer limits to their creativity. Figure (2.1) shows the Innoptus Solar Team vehicle, Infite, as an example of a solar vehicle.

Table 2.2: Top 3 teams for the last solar car competitions

Position	ASC 2022 (from [7])	WSC 2023 (from [8])
1	MIT (USA)	Innoptus Solar Team (Belgium) [9]
2	Principia (USA)	Solar Team Twente (Netherlands) [10]
3	Kentucky (USA)	Brunel Solar Team (Netherlands) [11]
Position	iESC 2022 (from [12])	ISC 2022 (from [13])
1	Sonnewagen Aachen (Germany)	Sonnewagen Aachen (Germany) [14]
2	Sonnewagen Aachen (Germany)	Solar Team Solaris (Turkey)
3	ITU (Turkey)	Solis (Romania)
Position	SCM 2021 (from [15])	SSC 2022 (from [16])
1	Solar Team Twente (Netherlands)	Brunel Solar Team (Netherlands)
2	Agoria Solar Team (Belgium)	Agoria Solar Team (Belgium)
3	Vattenfall Solar Team (Netherlands)	TUT Team (South Africa)

Figure 2.1: Innoptus Solar Team vehicle, Infinte.

The routes for each competition, as shown in 'my maps' [17], are based on data from the following sources [18], [19], [20], [21], [22], [23], and [24]. The iESC and ISC competitions are track-based, as shown in Figure (2.2), which illustrates the iLumen European Solar Challenge route in Belgium. The objective of track-based competitions is for teams to complete the maximum number of laps within a defined period, similar to what occurs in the Greenpower F24+. Meanwhile, the remaining solar competitions follow long-distance routes, as shown in Figure (2.3), which illustrates the route of the World Solar Challenge in Australia. The routes are divided into different segments, which can be completed over several days. The objective is to conclude all the segments as quickly as possible. For these long-distance route competitions, additional challenges are introduced, such as steep inclines and increased exposure to wind throughout the route.

Figure 2.2: iLumen European Solar Challenge track-based route, Belgium.

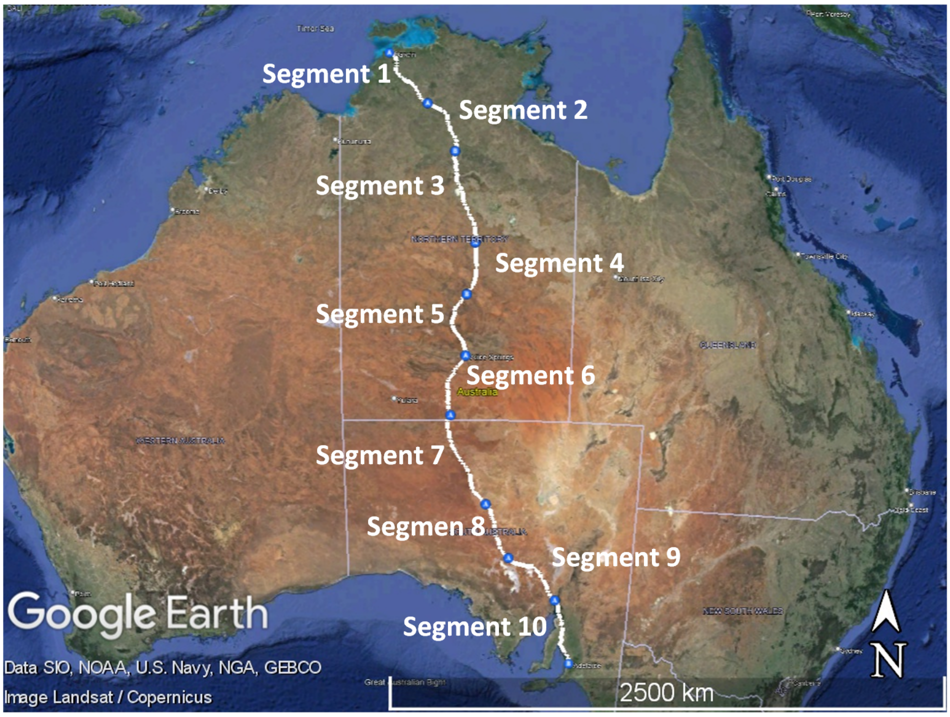

Figure 2.3: World Solar Challenge long-distance route, Australia.

It is evident that vehicles participating in solar competitions must have a considerable horizontal photovoltaic area in order to maximize energy production during the competition. The most common vehicle shape is that of a ”bullet,” which is designed to reduce aerodynamic drag and improve efficiency. With regard to the competitions themselves, long-distance routes present the most significant challenges due to the variations in altitude, irradiance, ambient temperature, and wind speed encountered along the routes. These factors underscore the importance of optimizing vehicle design and energy management strategies to adapt to the specific conditions of each competition.

3

Methodology

Contents

3.1 Introduction

In this chapter, the procedures conducted and considerations for the obtained results will be explained. The initial part of the procedure, outlined in section 3.2, involves conducting an initial analysis of environmental conditions, such as irradiance and temperatures, for various solar competitions. The aim is to investigate how these conditions affect the temperature and efficiency of photovoltaic cells.

Proceeding to the vehicle dynamics in section 3.3, which explains the forces applied to the vehicle, allowing the calculation of the power required for the vehicle to travel at a certain speed, enabling the calculation of the energy consumed by the vehicle.

The following section, section 3.4, focuses on the 1^{st} segments+ World Solar Challenge (WSC) and Solar Challenge Morocco (SCM) routes. It aims to obtain values for irradiance and ambient temperatures for various points along each track. Subsequently, the WSC is the focus of attention, as it is the most prestigious of the two competitions that the PSEM team wishes to concentrate on. The section then explains how to determine the vehicle's battery state of charge (SOC).

3.2 Environmental Analysis for Solar Competitions

In order to analyze the environmental conditions of each competition, the mean irradiance, G [W/m^2], and ambient temperature, T_{amb} [°C], values for the respective month of each competition are considered. Only data where solar radiation is present (i.e. when the irradiance values are different from 0) are included in the analysis. To do this, is used PVGIS through website [25], assuming an angle of inclination of 0 degrees for the photovoltaic cells. With this data, it is possible to obtain an average efficiency value for the photovoltaic cells for each of the competitions, verifying which ones make the best use of the cells.

Equation (3.1) demonstrates the methodology for estimating the temperature of photovoltaic cells, T_{cell} [°C], represented by T_{cell} [°C], utilizing a Nominal Operation Cell Temperature (NOCT) of 45°C. Assuming a monocrystalline solar cell from [26] with an area, A_{cell} [m^2], of 0.0156 m^2 and a peak power, P_p [Wp], of 2.8 Wp, it is possible to obtain the input power of the cell, P_{Cin} [W], with Equation (3.2). Through Equation (3.3), one can to compute the output power of the photovoltaic cell, P_{Cout} [W], to be determined taking into account the environmental conditions, considering a temperature coefficient, μ_{pp} [%], of -0.35 %, with an irradiance, G^r, equal to 1000 W/m^2 and a cell temperature, T^r, of 25°C. Finally, the cell efficiency, η [%], is obtained by dividing the output power by the input power of the solar cell, as it is represented in Equation (3.4).

The Equations (3.1), (3.2), (3.3) and (3.4) are utilized firstly to analyze the cells efficiency, temperature and power produced in each competition, which have different environments. Afterwards are necessary to estimate the power produced by the photovoltaic cells used in the vehicle, while the vehicle crosses the different segments of the selected competition, giving an idea of how much of the total energy consumption of the vehicle can be supplied by the cells.

$$T_{cell} = T_{amb} + \frac{G(NOCT - 20)}{800} \quad (3.1)$$

$$P_{Cin} = GA_{cell} \quad (3.2)$$

$$P_{Cout} = \frac{G}{G^r} P_p [1 + \mu_{pp}(T_{cell} - T^r)] \quad (3.3)$$

$$\eta = \frac{P_{Cout}}{P_{Cin}} \quad (3.4)$$

3.3 Vehicle Dynamics

3.3.1 Vehicle Linear Dynamics

Vehicle Linear Dynamics is the model proposed to determine the required torque of the electric vehicle when the environment changes by applying physical forces similar to the one used in [27]. So, the following forces are taken into account: aerodynamic drag force, F_d [N], traction force, F_t [N], frictional force, F_{roll} [N], and gravitational force component, $F_{\text{g}}{}'$ [N].

To understand how each force applied to the vehicle affects its motion, Figure (3.1) illustrates the forces acting on the vehicle. The vehicle is from Mobile Energy Sustainability Project (Projeto Sustentabilidade Energética Móvel) (PSEM) team's official website, from [28]. The 'x' axis represents the car's direction, while the 'y' axis is perpendicular to the ground, and φ is the road inclination.

It must be highlighted that, in the context of the vehicle's exclusive linear motion, forces beyond the 'x' axis of Figure (3.1) have not been considered. This excludes forces like the centripetal force experienced during a curve. The existent rotational dynamics in the car's wheel are the wheel rotational acceleration, α_w [rad/s^2], and the wheel rotational speed, ω_w [rad/s], which are directly related to the traction force, as previously mentioned, applied in the 'x' axis.

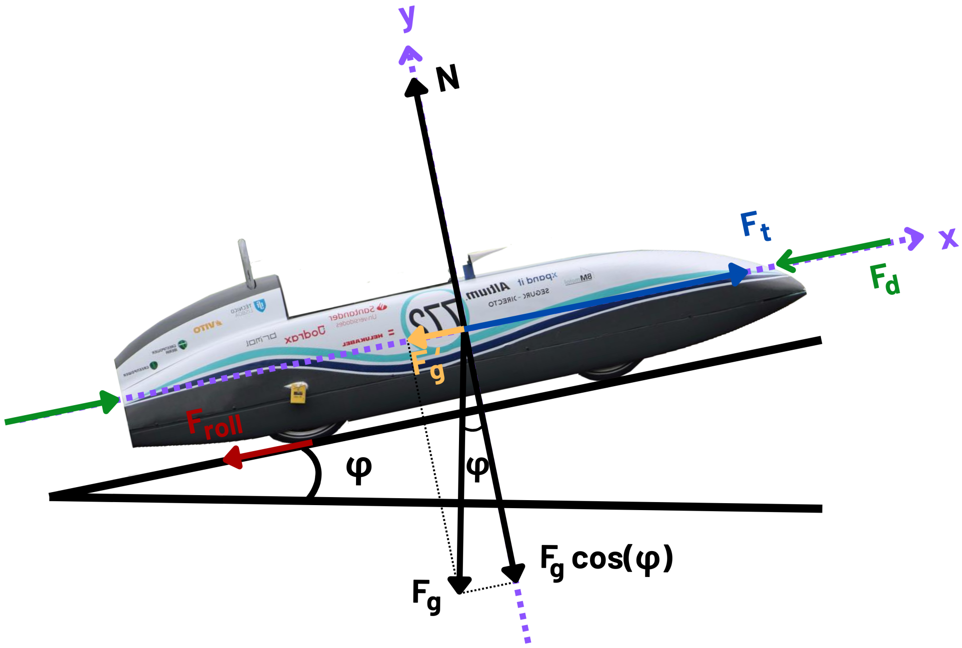

Figure 3.1: Physical forces applied to the vehicle.

Each force on the vehicle's motion, referred to in Figure (3.1), is characterized by the Equations below, incorporating the dynamics of linear forces (3.5) and (3.6), the aerodynamic drag force 3.7, the gravitational force component 3.8, the frictional force between the ground and the wheel 3.9, and the traction force described in Equation (3.10).

$$\sum F = M\frac{dv_c}{dt} \Leftrightarrow \tag{3.5}$$

$$\Leftrightarrow Ma = F_d + F_g' + F_t + F_{roll} \tag{3.6}$$

$$F_d = -\frac{1}{2}\rho_{air}C_dA_f[v_c - v_w\cos{(\theta)}]^2 \tag{3.7}$$

$$F_g' = -Mg\sin{(\varphi)} \tag{3.8}$$

$$F_{roll} = -|C_{rr}Mg\cos{(\varphi)}| \tag{3.9}$$

Starting with Equation (3.6), M [kg] is the total mass of the vehicle plus the driver, and a is the car acceleration.

For the aerodynamic drag force, denoted as F_d, it is crucial to acknowledge its dependency on the wind direction relative to the car. Here, ρ_{air} is equal to 1.225 [kg/m^3] representing the relative air density at 15℃, C_d is the drag coefficient, A_f [m^2] denotes the vehicle frontal area, v_c [km/h] is the vehicle speed, v_W [km/h] stands for the wind speed at 0.5 meters above the ground, and θ [°] represents the angle between the car and the wind. In Figure (3.1), two green vectors are illustrated, representing distinct wind directions. However, since aerodynamic drag is a resistive force, it opposes the movement of the vehicle and its absolute value increases if the wind opposes the vehicle's motion and decreases if the wind comes from the rear of the vehicle.

As mentioned earlier, only forces in the direction of the vehicle's movement are considered. Assuming that Figure (3.2) shows an upward view of the vehicle. The black dot represents the vehicle's center of mass, and the 'x' axis represents the direction of the vehicle's movement. The vector component of the wind velocity considered for the calculation of F_d is represented by a lighter green tone, $v_w \cos\theta$, which is in the same direction as the vehicle's movement, only changing its absolute value, between positive or negative depending on the environmental conditions.

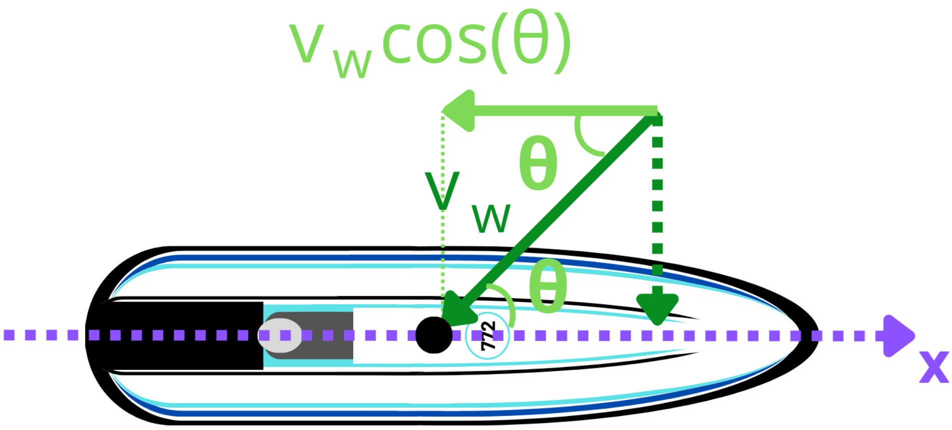

Figure 3.2: Wind vector influence.

Equation 3.8 calculates the component of the gravitational force applied to the vehicle along the 'x' axis, where φ [°] represents the inclination angle of the road, and g is the acceleration due to gravity [m/s^2].

The Equation (3.9) considers the friction between the ground and the wheel during the vehicle's movement, signifying that the frictional force always opposes the direction of the vehicle's motion. The variable C_{rr} is the coefficient of rolling resistance.

3.3.2 Vehicle Rotational Dynamics

The subsequent step involves determining the car's traction torque and then calculating the power required for the car to achieve the desired speed. To achieve this, it is necessary to obtain the traction force F_t. Figure (3.3) illustrates the physics behind the vehicle's wheel.

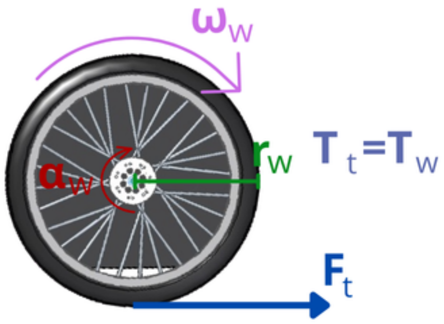

Figure 3.3: Physic dynamics for the wheels of the car.

The Equation (3.6) represents the linear aspect of the vehicle's motion. The rotational aspect of its movement is depicted in Equation (3.10). Rewriting the equation results in F_t, where I_t [kg·m^2] represents the inertia of the rotational parts of the vehicle, T_t [Nm] is the traction torque, r_w [m] is the wheel radius, and ω_w and α_w have been previously introduced.

$$\begin{cases} I_t\alpha_w = T_t - F_t r_w \Leftrightarrow I_t\frac{d\omega_w}{dt} = T_t - F_t r_w \\ \Rightarrow F_t = \frac{T_t}{r_w} - \frac{I_w\alpha_w}{r_w} \end{cases} \tag{3.10}$$

By replacing the Equation (3.10) in Equation (3.6), it is possible to determine the traction torque T_t and then the power needed by the vehicle to travel at the desired speed. The Equations, (3.11), (3.12), (3.13) and (3.14) below show all the procedures to do this. The Equation (3.12), of the equivalent total mass of the vehicle, M_{eq} [kg]. Has the variable,f_m, that represents the mass factor.

$$\alpha_w = \frac{a}{r_w} \tag{3.11}$$

$$M_{eq} = M + \frac{I_w}{r_w^2} = Mf_m \tag{3.12}$$

$$\begin{cases} Ma = F_d + F_g' + \left(\frac{T_t}{r_w} - \frac{I_w\alpha_w}{r_w}\right) + F_{roll} \Leftrightarrow Ma + \frac{I_w\alpha_w}{r_w} = F_d + F_g' + \frac{T_t}{r_w} + F_{roll} \Leftrightarrow \\ \Leftrightarrow \left(M + \frac{I_w}{r_w^2}\right)a = F_d + F_g' + \frac{T_t}{r_w} + F_{roll} \Leftrightarrow T_t = \left(M_{eq}a - F_d - F_g' - F_{roll}\right) r_w \end{cases} \tag{3.13}$$

$$P_t = T_t\omega_w \tag{3.14}$$

Using the traction power, P_t, one can calculate the energy consumed during a specific route.

3.4 Environmental Conditions Analysis for the First Segments of the Solar Challenge Morocco and World Solar Challenge

Subsequent to the environmental conditions study in section 3.2, is decided to concentrate the analysis on SCM competition. This decision is influenced by the proximity of this competition regarding the time required for project completion. After discussions with the PSEM team, we opted to prioritize the study of the WSC first, as the team's objective is to participate in this competition as soon as possible, but this decision is made only after obtaining some results for the SCM. Therefore, the entire process for SCM occurred before any process for WSC commenced, which started only after the discussion with the PSEM team. Throughout the procedure below, both competitions will be involved in the steps carried out for each, highlighting the differences in procedures. However, eventually, the focus of the procedure will shift exclusively to the WSC, since it is also the competition with the most prestige.

The first step is to divide the routes of SCM and WSC into segments, enabling the acquisition of results with a reduced amount of data, making it more straightforward to scrutinize the methodology employed. These segments are categorized based on the control stop locations of the routes for each competition. The segments of SCM can be accessed through the official competition website (from [19]), with a hyperlink available on the site leading to this link (from [29]). As for WSC, each segment is mapped on the following "My Maps", [30], based on the provided route details (from [18]).

Subsequently, it is decided to select the initial segment of each competition and gather irradiance and temperature data every 25 km along the track. For SCM, the data is collected using PVGIS. In the case of WSC, it is opted to acquire data every 10 km to enhance precision in the analysis, resulting in a total distance of 323 km for the first segment. The datasets encompass hourly irradiance and temperature values for SCM from 2015 to 2020 and for WSC from 2005 to 2020, sourced from the 'hourly data' section (from [25]).

Based on these data, the study continued exclusively for the first segment of WSC. Proceeding to obtain the altitude values for each point along the route relative to the sea level is obtained using Google Earth. By utilizing the [31] website, it is obtained both wind speed values at an altitude of 10 meters and their corresponding directions. Applying Prandtl's Law in Equation (3.15) allows us to estimate the wind speed at an altitude of 0.5 meters above the ground. in order to accomplish this, the surface roughness length (Z_0) is determined by observing the amount of buildings and vegetation in the surrounding area at each track point. Multiple tables with (Z_0) values are consulted to ensure accuracy, given the similarity of values among them, although none of the tables are equal.

$$v_w = \frac{\ln\left(\frac{Z_w}{Z_0}\right)}{\ln\left(\frac{Z_{w10m}}{Z_0}\right)} v_{w10m} = \frac{\ln\left(\frac{0.5}{Z_0}\right)}{\ln\left(\frac{10}{Z_0}\right)} v_{w10m} \tag{3.15}$$

3.5 World Solar Challenge Analysis

The analysis focuses on the World Solar Challenge competition, as previously mentioned. Establishing the speed at which the vehicle will proceed through each competition segment is essential. The vehicle must maintain a minimum speed of 60 km/h, since a speed below this threshold will result in the vehicle being trailered to the next mandatory control stop and consequently prevented from continuing on any further segments. Therefore, it is determined that the vehicle will travel the WSC competition at a speed of 70 km/h.

With the vehicle's speed set, it is now possible to plan how it will cover the competition's segments. Table (3.1) provides the distances needed to cover for each segment and also an easier view of how the competition is conducted, when the vehicle travels at a speed of 70 km/h, allowing it to complete the competition within seven days. To achieve this, the vehicle must complete two segments of the competition in a single day, more than once. Accordingly, as each day of the competition commences at 8h and concludes at 17h, the duration of each competition day is 9 hours. Given that a 30-minute stop is required after each segment, the vehicle can be in motion for 8 hours and 30 minutes per day. It is decided that the first and second segments would be covered on 13 October. Given the considerable length of the third segment, completing another segment on the same day is impossible. The schedule is designed with the objective of enabling the vehicle to conclude the competition as quickly as possible at a speed of 70 km/h.

Consequently, the third segment will be completed on 14 October. Segments four and five are scheduled for coverage on October 15. On 16 October, only the sixth segment will be covered, as the seventh is the longest segment and will require a full day on its own on 17 October. The eighth and ninth segments will be covered on 18 October, and finally, the last segment, the tenth, will be completed on 19 October. As a result, the competition is scheduled to be concluded on October 19, one day before its final deadline.

Table 3.1: Distance covered and corresponding day for each World Solar Challenge competition segment.

Day of October	13		14	15		16	17	18		19
Segment	1	2	3	4	5	6	7	8	9	10
Distance [km]	324	267	401	222	285	273	413	254	289	306

By gathering the route coordinates for each segment of the competition and their altitude variations, each segment's irradiance, ambient temperature, and wind speed can be obtained according to the planned schedule. These values are provided every 10 km for all hours between 8 and 17 hours, similar to what was done for the first segment of the competition. The approximations are obtained through the use of cubic interpolation, with a distance interval of 250 meters between each point, and a time interval of 36 seconds. However, these intervals can be modified according to the specific necessities of the user. These intervals are chosen to reduce the difference in values from one point to the next within the segment for each data set approximation. Figure (3.4a) shows the original data for the irradiance, while Figure (3.4b) illustrates the approximation obtained utilizing the time and distance intervals mentioned before.

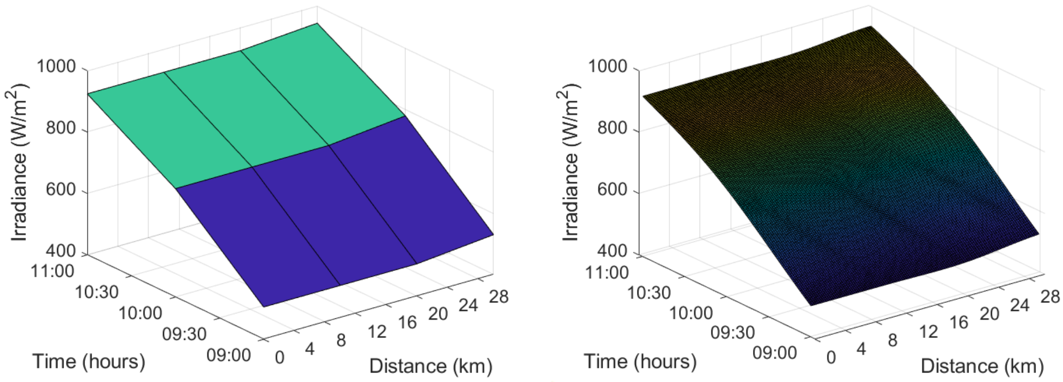

(a) Irradiance curve without approximation. **(b)** Approximation of the irradiance curve.

Figure 3.4: Approximation for the first segment of the World Solar Challenge.

With all the data obtained, it is necessary to specify the vehicle parameters to calculate the power generated by the installed array of panels, as well as the power required at the vehicle's wheel, thereby allowing the energy supplied by the battery pack to be determined. These parameters are listed in Table (3.2), where C_{rr} is the rolling resistance coefficient, f_m is the mass factor, M is the total mass of the vehicle plus the driver, C_d is the aerodynamic drag coefficient, A_f is the vehicle's frontal area, r_w is the vehicle's wheel radius, A_{PV} is the panel array area, P_p is the panel's peak power, and u_{pp} is the temperature coefficient. Additionally, the electrical and mechanical configuration obtained by António Faria is presented in Figure (3.5), and the efficiency data provided in Table (3.3) are taken into account for the numerical model, the solar cells used are the Maxeon Gen III, X-series from [32].

Table 3.2: Vehicle parameter assumptions.

C_{rr}	f_m	M [kg]	C_d	A_f [m^2]	r_w [m]
0.0051	1.05	142.5	0.10	0.45	0.225
Battery capacity [Wh]			A_{PV} [m^2]	P_p [W]	u_{pp} [%/°C]
5600			1.58	353.7	-0.3

Figure (3.5) it also illustrates the vehicle's power flow. The solid arrows represent the electrical power flow, while the rectangle with an arrow represents the mechanical power flow. The dashed arrows indicate the potential of regenerating electrical power flow, such as when the vehicle travels downhill. This configuration enables the photovoltaic panels to provide energy without going through the battery, reducing power loss and avoiding unnecessary charging time. The excess is stored in the battery if the photovoltaic panels produce more energy than needed. If the output power of the panels is insufficient, the battery supplements the required power.

Figure (3.5) also illustrates the vehicle's power flow. The solid arrows represent the electrical power flow, while the rectangle with an arrow indicates the mechanical power flow. The dashed arrows represent the potential for regenerating electrical power, such as when the vehicle travels downhill. This configuration allows the photovoltaic panels to supply energy directly to the vehicle without passing through the battery, reducing power loss and avoiding unnecessary charging time. The excess is stored in the battery if the photovoltaic panels produce more energy than needed. If the output power of the panels is insufficient, the battery supplies the remaining required power.

Table 3.3: Efficiency considered for the elements of the Figure (3.5).

Segment	Battery	Charge controller	DC/DC Converter	Motor	Gearbox
Efficiency [%]	85	85	85	75	85
Quantity	1	1	1	1	1

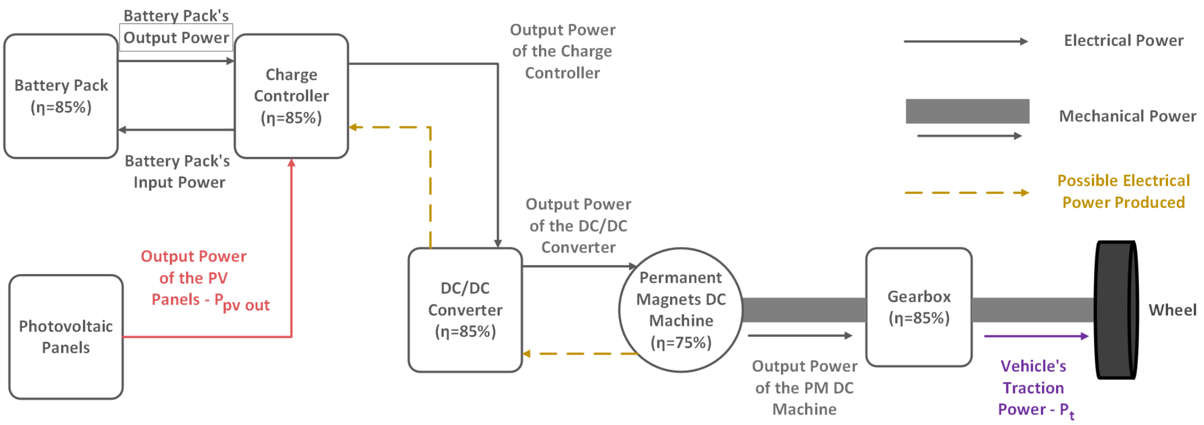

Figure 3.5: Electrical/Mechanical configuration considered for the vehicle, η is the equipment's efficiency.

With all the required data available for the simulation of each segment. Figures (3.6) and (3.7) present a diagram elucidating the operational mechanics of the vehicle numerical model. It follows the steps explained in the methodology to calculate the output power of the photovoltaic panel array, the power required by the vehicle traveling at a speed of 70 km/h, and, consequently, the power provided by the battery. Furthermore, the battery's state of charge (SOC) after the segment and the requisite completion time are determined. Additionally, the numerical model indicates the time and battery percentage with which the vehicle initiates the next segment for the days that it is scheduled.

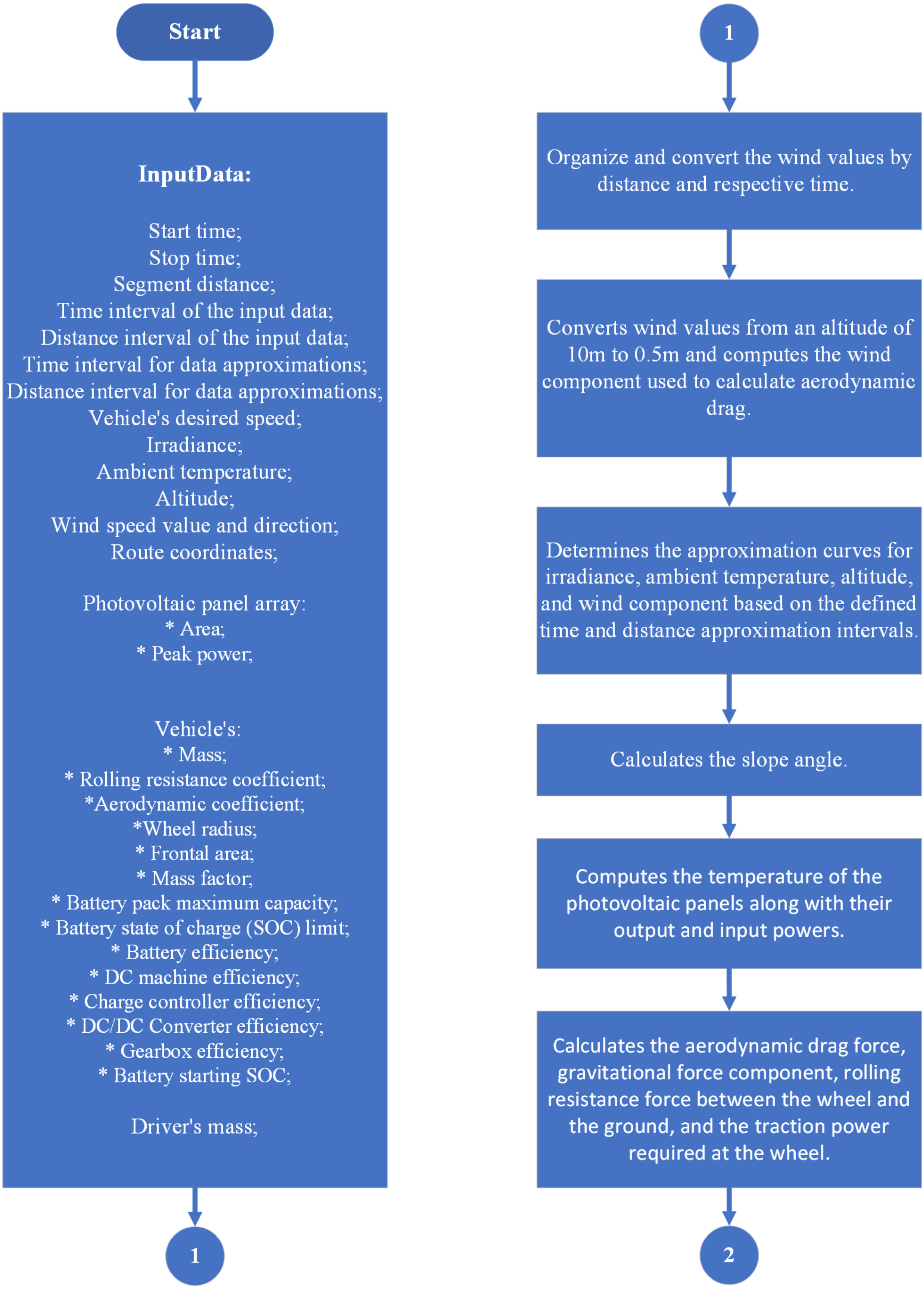

Figure 3.6: Diagram 1, explaining the operation of the numerical model.

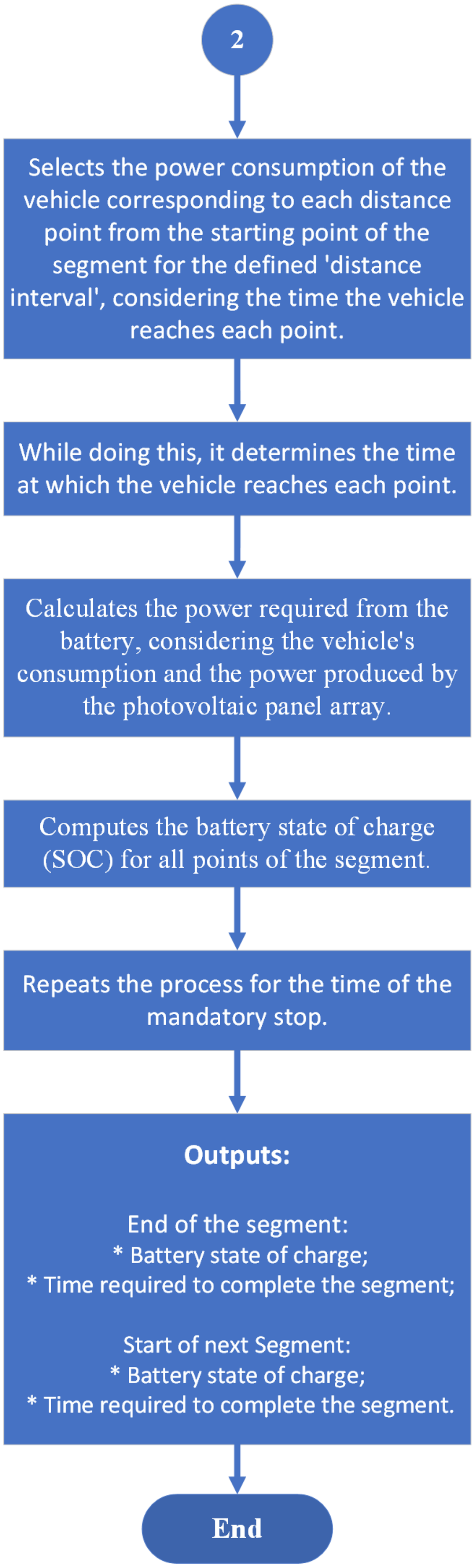

Figure 3.7: Diagram 2, explaining the operation of the numerical model.

4

Results

Contents

4.1 Results of Environmental Analysis for Solar Competitions of Section 3.2

The color-coded separation in Table (4.1) clarifies the information presented in Table (4.2). The points selected for Table (4.2) are shown in the following link [33]. Analyzing this table, one can observe that the iLumen European Solar Challenge (iESC) and Italian Solar Challenge (ISC) competitions maintain consistent conditions throughout their courses, as they take place on Formula 1 tracks. When comparing all competitions based on their monthly average irradiance values, it becomes evident that Carrera Solar Atacama (CSA) exhibits the highest values, followed by World Solar Challenge (WSC) and Sasol Solar Challenge (SSC), while both ISC and iESC present lower average irradiance values. It is worth noting that the Solar Challenge Morocco (SCM) competition stands out for maintaining the most constant irradiance values throughout its course, while American Solar Challenge (ASC) is the competition where the values change the most.

Cell temperatures are considered for the analysis of monthly average temperatures, as they depend on ambient temperature and are influenced by the irradiance to which the cells are exposed. It is observed that iESC has the best temperature, being very close to T^r, 25 ºC. Competitions SCM and ISC also present low temperature values. For the CSA, WSC and ASC competitions it is noted that temperature values vary significantly across their zones, in the case of ASC, and routes, in the case of CSA and WSC. ASC exhibits the greatest temperature variation, including the worst values. However, it is worth remembering that in the case of this competition, the route does not cover all zones, only some that change from competition to competition depending on the route chosen for that year.

Observing the efficiency values, it is clear that ASC and WSC exhibit the lowest efficiencies, with values below 17% for the majority of the points. Both have an average efficiency value for their points of 16.8%. On the other hand, the competitions ISC, SSC, CSA, and SCM present their respective averages, 17.3%, 17.2%, 17.2%, and 17.4%, being values quite close. For CSA, the efficiency values show a significant variation during the track, mainly due to the cell temperatures having a large difference from one point to another, reaching an efficiency below 17% at the first point. In the case of SCM, there is a variation in efficiencies, but their values are always above 17%. The iESC stands out with the best efficiency value.

There is an evident difference of 1.9% between the highest and lowest efficiency values; however, since average values are employed in the study, this difference is mitigated. When more reliable data is used, the contrast between the maximum and minimum efficiency tends to increase, and the same trend applies to the variations between points within the same competition. Despite this, it is chosen to focus the future analysis in the WSC, since it is the most prestigious competition, being the one that the PSEM team prefers, showing the second highest average solar cell power output of 1.4 W.

Table 4.1: Color visual representation for Table (4.2).

G [W/m²]	Worst	$G < 400$	$G \geq 400$	$G \geq 450$	$G \geq 500$	$G \geq 600$	Best
T_{cell} [ºC]	Worst	$T_{cell} > 45$	$T_{cell} \leq 45$	$T_{cell} \leq 40$	$T_{cell} \leq 35$	$T_{cell} \leq 30$	Best
η_{cell} [%]	Worst	$\eta_{cell} < 16.5$	$\eta_{cell} \geq 16.5$	$\eta_{cell} \geq 17$	$\eta_{cell} \geq 17.5$	$\eta_{cell} \geq 17.7$	Best

Table 4.2: Analysis for Solar Competitions from 3.2, the letters represent the sun hours for each condition, a) 5:30h - 17:30h, b) 5:30h - 18:30, c) 5:30h - 19:30h, d) 6:30h - 17:30h, e) 6:30h - 18:30h, f) 6:30h - 19:30h.

Comp	Local	Month	G [W/m²]	T_{amb} [ºC]	T_{cell} [ºC]	P_{Cin} [W]	P_{Cout} [W]	η_{cell} [%]
ASC	DDS c)	7	458	22.1	36.41	7.15	1.23	17.2
	DDS c)	8	386	20.9	32.96	6.03	1.05	17.4
	DAL c)	7	450	31.3	45.36	7.03	1.17	16.6
	DAL e)	8	484	31.6	46.73	7.56	1.25	16.6
	GEO f)	7	435	29.9	43.53	6.80	1.14	16.8
	GEO e)	8	418	30.3	43.34	6.53	1.09	16.8
	IDA c)	7	496	30.3	45.77	7.75	1.29	16.6
	IDA c)	8	427	19.0	32.32	6.67	1.16	17.5
	LAV b)	7	563	37.8	55.40	8.80	1.41	16.0
	LAV b)	8	523	36.5	52.86	8.18	1.32	16.2
	OHI c)	7	411	23.3	36.18	6.42	1.11	17.2
	OHI c)	8	363	22.1	33.40	5.67	0.99	17.4
WSC	ADE a)	10	488	20.8	36.01	7.63	1.31	17.2
	ALS a)	10	552	26.1	43.37	8.63	1.45	16.8
	COP a)	10	526	25.4	41.87	8.22	1.39	16.9
	DAR f)	10	570	30.6	48.36	8.90	1.46	16.5
	PAM a)	10	555	31.1	48.48	8.67	1.43	16.4
iESC	CZ e)	9	248	17.6	25.40	3.88	0.69	17.9
ISC	AEDF e)	9	324	24.2	34.33	5.07	0.88	17.3
SSC	BRI d)	9	510	18.5	34.39	7.97	1.38	17.3
	NCT d)	9	468	25.0	39.60	7.32	1.24	17.0
CSA	ANT e)	10	653	25.7	46.15	10.20	1.69	16.6
	ARI e)	10	510	19.7	35.65	7.97	1.37	17.3
	CAL e)	10	651	17.9	38.26	10.17	1.74	17.1
	CPÓ e)	10	610	20.7	39.78	9.53	1.62	17.0
	IQU e)	10	601	20.0	38.84	9.40	1.60	17.1
	LAS e)	10	541	14.9	31.85	8.46	1.48	17.5
	SPE e)	10	563	14.7	32.25	8.79	1.54	17.5
	SAN e)	10	498	18.5	34.01	7.78	1.35	17.4
SCM	1D2 d)	10	427	15.1	28.42	6.67	1.18	17.7
	1D4 d)	10	438	23.5	37.21	6.84	1.17	17.2
	2D1 d)	10	428	17.9	31.27	6.69	1.17	17.5
	2D3 d)	10	422	15.8	29.01	6.59	1.16	17.7
	2D5 d)	10	430	22.6	36.07	6.72	1.16	17.2
	3D2 d)	10	420	19.7	32.83	6.57	1.14	17.4
	3D4 d)	10	427	22.6	35.94	6.67	1.15	17.2
	4D1 d)	10	431	23.4	36.92	6.74	1.16	17.2
	4D3 d)	10	418	20.0	33.06	6.54	1.14	17.4
	4D5 d)	10	432	21.8	35.27	6.75	1.17	17.3

4.2 Results for the First Segments of Solar Challenge Morocco and World Solar Challenge

Using data from 10/25/2015, considering that the segment for the first day of SCM in 2021, which is covered on 10/25/2021, the following data is obtained for Figures (4.1b), (4.1a), (4.1c) and (4.1d). These depend on the distance covered during segment 1, considering at what time the vehicle passes each point of the track.

In Figure (4.1b) is illustrated the irradiance levels throughout the course. It is notable that, during the majority of the journey between 10h and 15h, irradiance levels surpass 400 W/m^2. Additionally, lower values are observed in the initial and middle sections of the segment, while the final segment exhibits the highest irradiance levels. Figures (4.1a) and (4.1c) depict the variations in ambient temperature and cell temperature, respectively. Upon comparison, a parallel behavior is evident along the track. The cell temperature records higher values, influenced not only by ambient temperature but also by the irradiance to which the cell is exposed, as described in Equation (3.1), for Nominal Operation Cell Temperature (NOCT) equal to 45ºC. Similar temperatures are noted from 0 km to 100 km and from 300 km to 475 km, with temperatures exceeding 40℃ at 475 km. A significant temperature decrease is observed between 100 km and 300 km on the track, with this decline being more gradual in cell temperature. For Figure (4.1d), Equation (3.3) is adjusted to be independent of the cell's peak power. To achieve this, as expressed in Equation (4.1), the cell's peak/maximum power is not multiplied, denoted as P_p. Figure (4.1d) represents the percentage of the maximum power that the cell provides for different temperature and irradiance values when compared the maximum power that the cell produces with an irradiance of 1000W/m^2 and cell temperature of 25℃, G^r and T^r.

$$P_{Cout}/P_{max} = \frac{G}{G^r}[1 + \mu_{pp}(T_{cell} - T^r)] \tag{4.1}$$

Figure (4.1d) exhibits a behavior very similar to Figure (4.1b). The decrease in values presented for irradiance is slightly attenuated in Figure (4.1d), as the lower cell temperature values coincide with those of irradiance in the middle of the track. It is important to highlight that during the majority of the route, cells produce less than 60 %. Through this analysis, one can deduce that, at the beginning and between the 200 km and 300 km marks, the vehicle should traverse those segments more quickly than the rest of the segment, thereby maximizing the utilization of energy generated by the photovoltaic cells.

Similar to the approach taken for Figure (4.1d), Figure (4.2d) follows the same reasoning. It is observed that for some values, the power produced by the cell reaches 90% of its maximum power. This is attributed to some irradiance values at certain points in the segment exceeding 1000 W/m^2. Additionally, it is noted that, for this course, photovoltaic cells are expected to produce less power in the first 100 km.

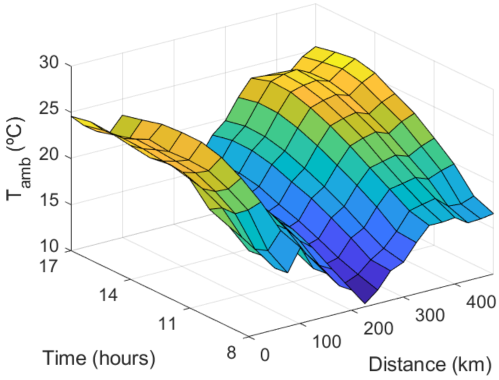

(a) Ambient temperature values along segment 1 of Solar Challenge Morocco.

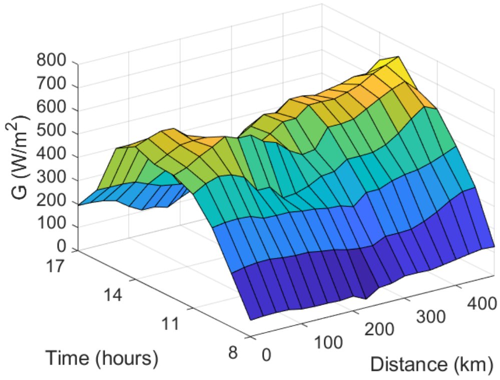

(b) Irradiance values along segment 1 of Solar Challenge Morocco.

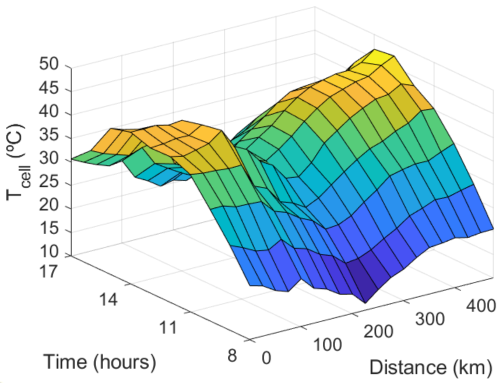

(c) Cell temperature values along segment 1 of Solar Challenge Morocco.

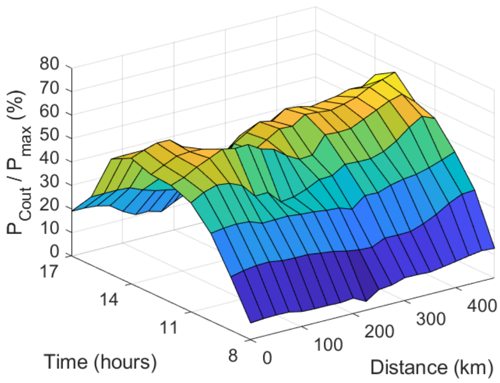

(d) P_{Cout} / P_{max} along segment 1 of Solar Challenge Morocco.

Figure 4.1: Segment 1 of Solar Challenge Morocco.

Focusing on the WSC Figures, is utilized data from the competition on October 13, 2019. Using the same methods as for SCM are obtained the Figures (4.2a) and (4.2c), which illustrate temperature values with minimal fluctuations throughout the course, particularly for cell temperatures. Ambient temperatures before the 50 km mark are notably lower. It's worth noting that the observed cell temperature values follow a different curve than ambient temperature values, due to the high irradiances that the cells experience throughout the entire segment. Interestingly, this competition demonstrates higher temperature values compared to SCM. The acquisition of cell temperatures is conducted in the same way as in the previous competition. In Figure (4.2b), it is notable that irradiance values surpass those in Figure (4.1b), reaching levels close to 1000 W/m^2 around 12h to 13h in the second half of the journey, with slightly lower values for the first half.

The Figure (4.3a), shows the altitude variations for the first segment of the WSC. Represented in Figure (4.3b) is the wind speed values for each distance point of the segment at a specific hour, relative to the vehicle's direction of movement referred in Section 3.4. It is shown that during the first segment route, the wind will change significantly, affecting the vehicle's performance.

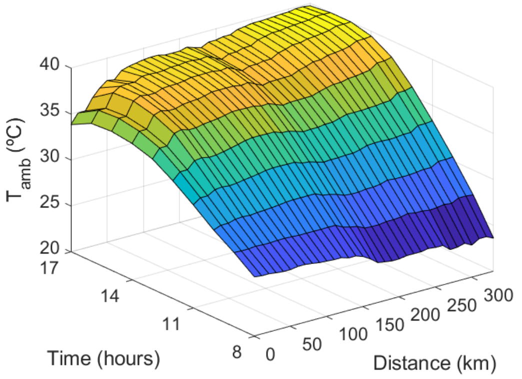

(a) Ambient temperature values along segment 1 of World Solar Challenge.

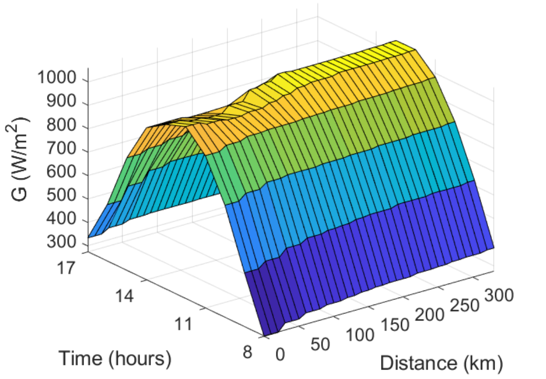

(b) Irradiance values along segment 1 of World Solar Challenge.

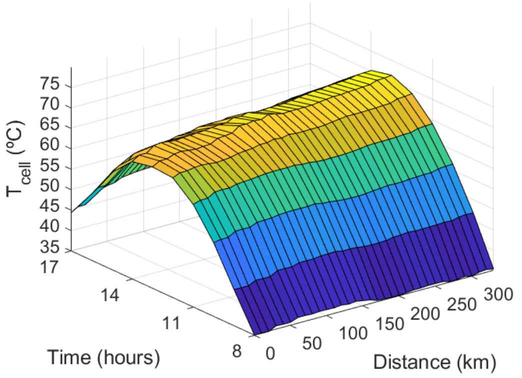

(c) Cell temperature values along segment 1 of World Solar Challenge.

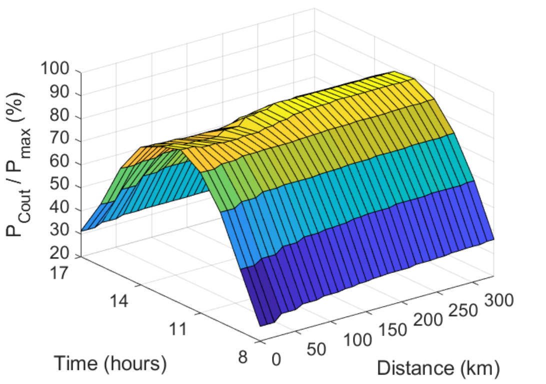

(d) P_{Cout} / P_{max} along segment 1 of World Solar Challenge.

Figure 4.2: Segment 1 of World Solar Challenge.

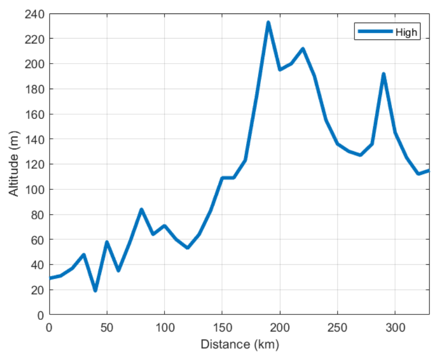

(a) Altitude for the first Segment of World Solar Challenge.

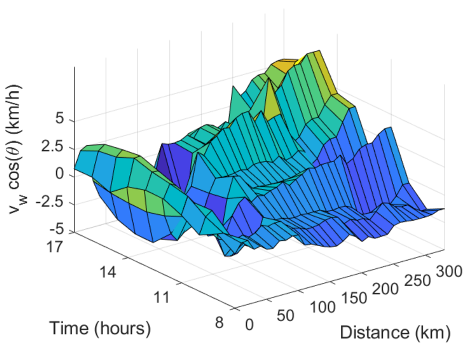

(b) Wind speed for the first segment of the World Solar Challenge.

Figure 4.3: Altitude and Wind speed for the first segment of the World Solar Challenge.

4.3 World Solar Challenge Environmental Conditions Results

From this section onwards, the results obtained for the World Solar Challenge over seven days are demonstrated, where the vehicle follows the competition route, confirming that the planned schedule is successfully executed. This section analyzes the environmental conditions to which the vehicle is exposed during the competition based on the data obtained with more detail. The aim is to identify any patterns that may be repeated in the future for this competition. The environmental conditions considered include ambient temperature, irradiance values, wind speed, and altitude variations throughout the competition segments. The process of data collection and application during this phase proved to be challenging due to the necessity of intermediate steps that had to be carried out for its implementation in the numerical model.

To begin, Figure (4.4) illustrates the parts of the route traveled during each day of the competition, helping to understand the analysis of ambient temperature, irradiance, and wind speed discussed ahead. From a preliminary analysis, it is observed that the route can be divided into three zones: the 1st, 2nd, and 3rd segments are zones with more vegetation, representing zone 1; from segments 4 to 9, the route passes through a desert, zone 2; and the 10th segment is also in a zone with more vegetation zone 3. While the vehicle crosses zone 2, it is possible to present an additional difficulty since the vehicle may be more exposed to the wind.

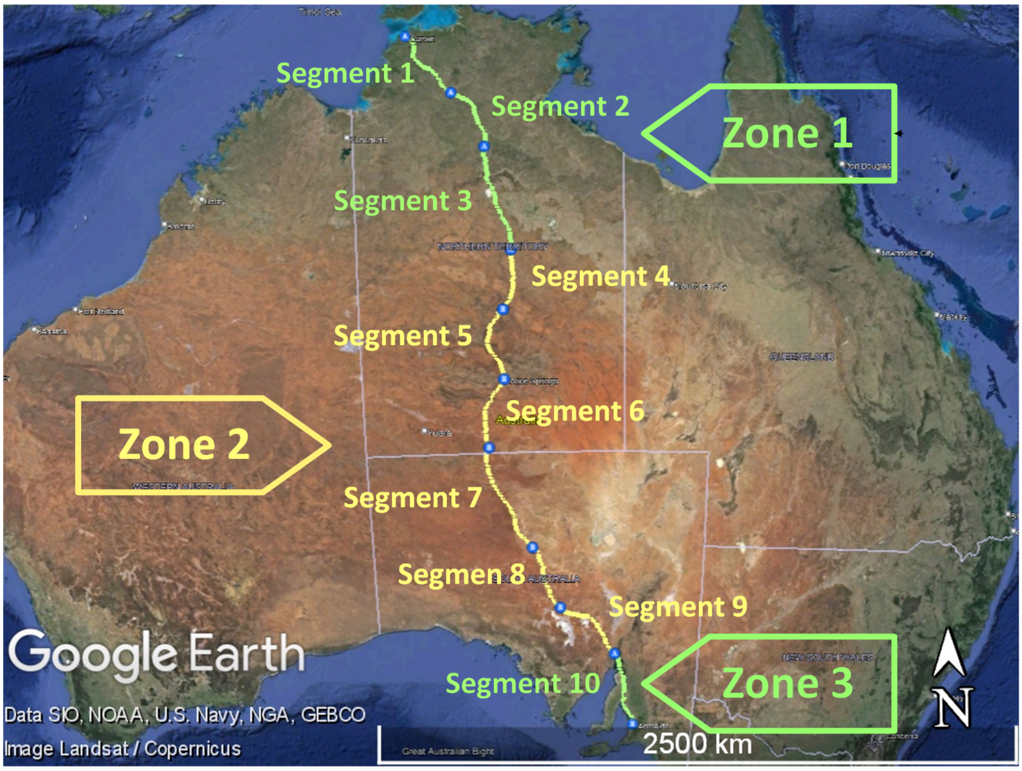

Figure 4.4: Environments across the World Solar Challenge route.

4.3.1 Ambient Temperature

Starting with the Ambient temperature, the Figures (4.5) and (4.8) demonstrates the variation in ambient temperature to which vehicle is exposed to while crossing the segments designated for each day of the competition. It can be observed that in the initial three days (October 13th, 14th and 15th), for segments 1, 2, 3, 4, and 5, the temperatures exhibited a consistent pattern throughout the day, starting at 25 ℃ to slightly above for the 3 days. Furthermore, the temperature reached almost 40 ℃ for the first three days. In the fifth segment, the ambient temperature decreases to approximately 37 ℃, after reaching its peak value. Additionally, some irregularities are observed, which are likely attributed to cloudy conditions. During these first three days, there exists a daily increase of the ambient temperature of around 15 ℃, which also suggests a warm environment. On the fourth day (October 16th), is observed a decrease in temperature, coinciding with segment 6. The temperature variation is lower compared to the previous days, with an initial temperature of around 24 ℃ and a peak around the 27 ℃, demonstrating a smaller range of temperature fluctuation. The fifth day(October 17th), shows lower temperature values with an initial temperature of 15 ℃, reaching the approximately 23 ℃. Resulting in a considerable temperature variation. During the sixth day of the competition (October 18th), when segments 8 and 9 are covered, there is a temperature variation of more than 10 ℃, with higher temperature values than on the previous day, Reaching values around the 27 ℃. On the final day (October 19th), the 10^{th}segment is transversed, demonstrating a temperature variation of less than 5 ℃, showing the lowest temperature values. The observed temperature variations are consistent with the movement of the vehicle, as the route traversed from north to south across Australia is expected to result in a decrease of temperature.

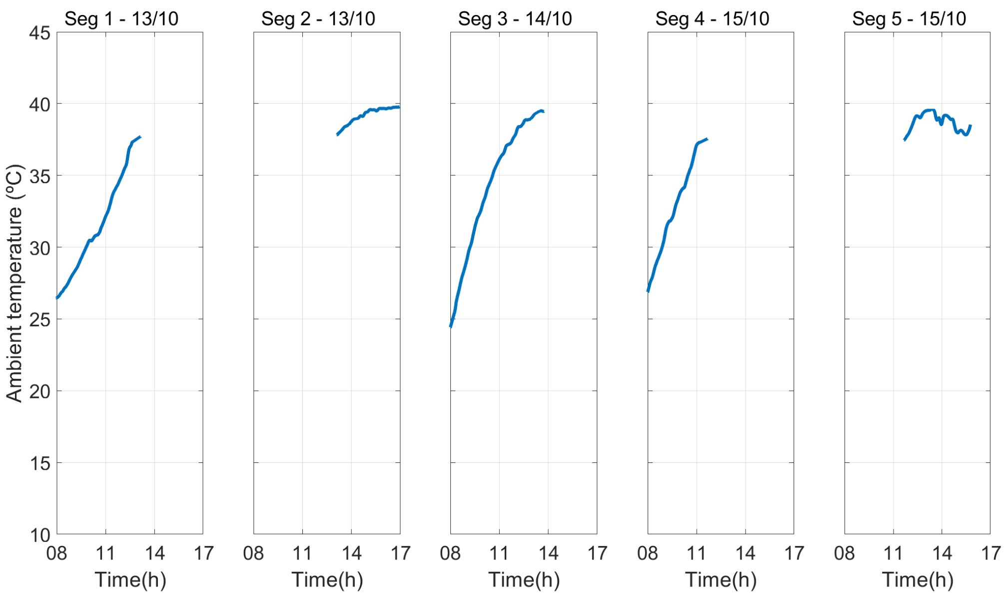

Figure 4.5: Ambient temperature throughout the 1^{st} and 5^{th} segments.

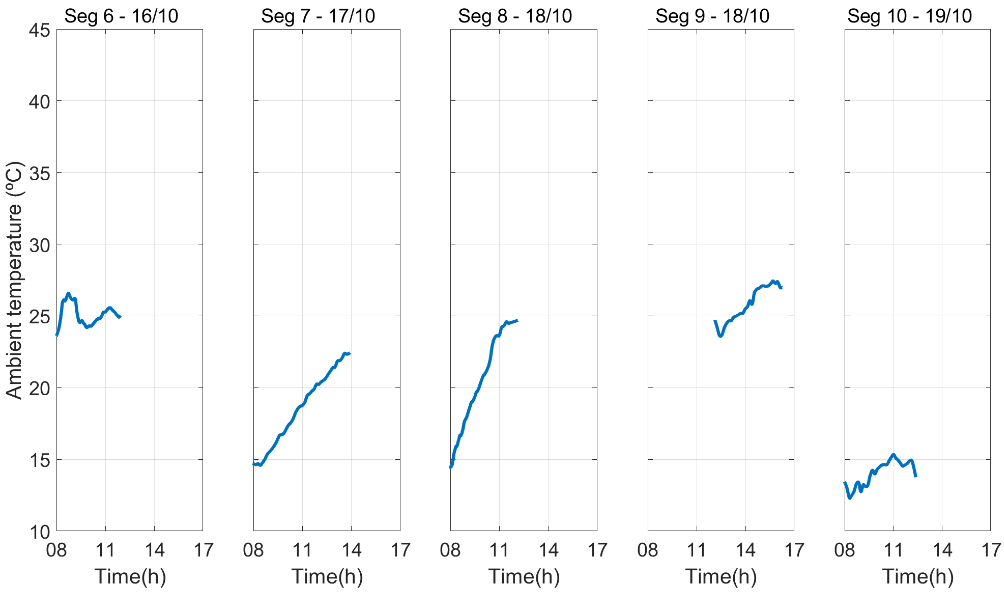

Figure 4.6: Ambient temperature throughout the 6th and 10th segments.

4.3.2 Irradiance

Moving on to the analysis of irradiance, Figures (4.7) and (4.8) display the irradiance values over time as the vehicle travels through each segment. This irradiance values demonstrate a consistent pattern over the course of the day, with the exception of the third, fourth, and final day, during the fifth, sixth, and tenth segments, respectively. The presence of cloud cover during the fifth and sixth segments resulted in the obstruction of sunlight, thereby giving rise to irregularities in the irradiance curve. This phenomenon is also observed at the end of the fourth segment, although to a lesser extent than in the other two segments, being relatively irrelevant. In the tenth segment, a decrease and irregularities in the irradiance curve are evident, which may have been due to a change in weather compared to the previous days, or simply cloudier conditions. Furthermore, it is evident that on all but the final day, the irradiance exceeded 1000 W/m^2. On the final day, the highest value observed reached approximately 700 W/m^2, it is possible that this happen due to this day the weather, being an example of a possible worst case scenario. As with the ambient temperature, the irradiance values show a decline as the vehicle moves towards the southern Australian region, with the greatest reduction occurring on the final day. It is expected that the energy production from the photovoltaic panels will be lower than that generated on previous days. To demonstrate how the energy produced by the panels is likely to decline in comparison to the other days of the competition, it is useful to consider the impact of unfavourable weather conditions.

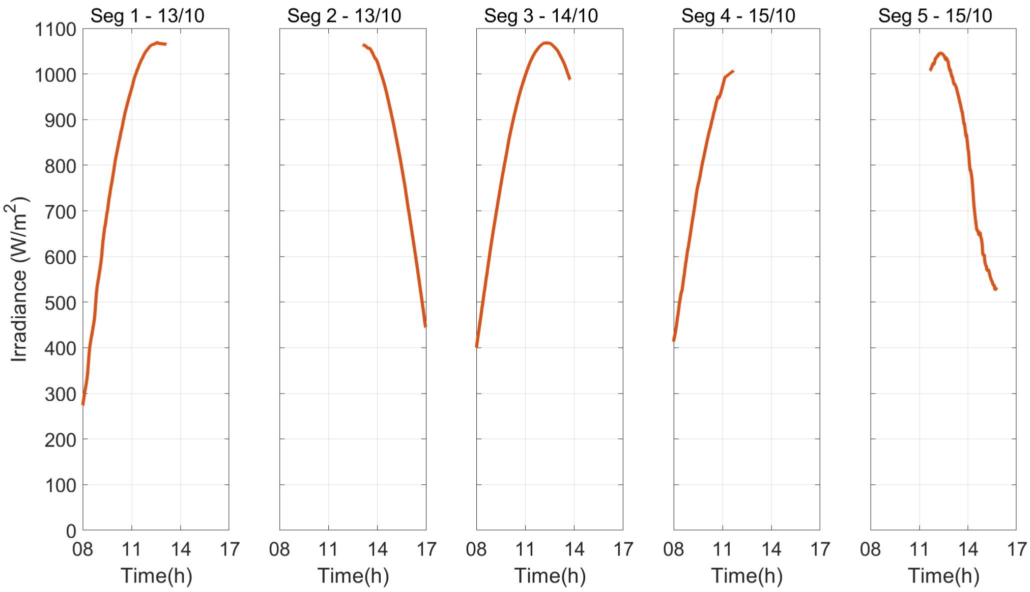

Figure 4.7: Irradiance throughout the 1^{st} and 5^{th} segments.

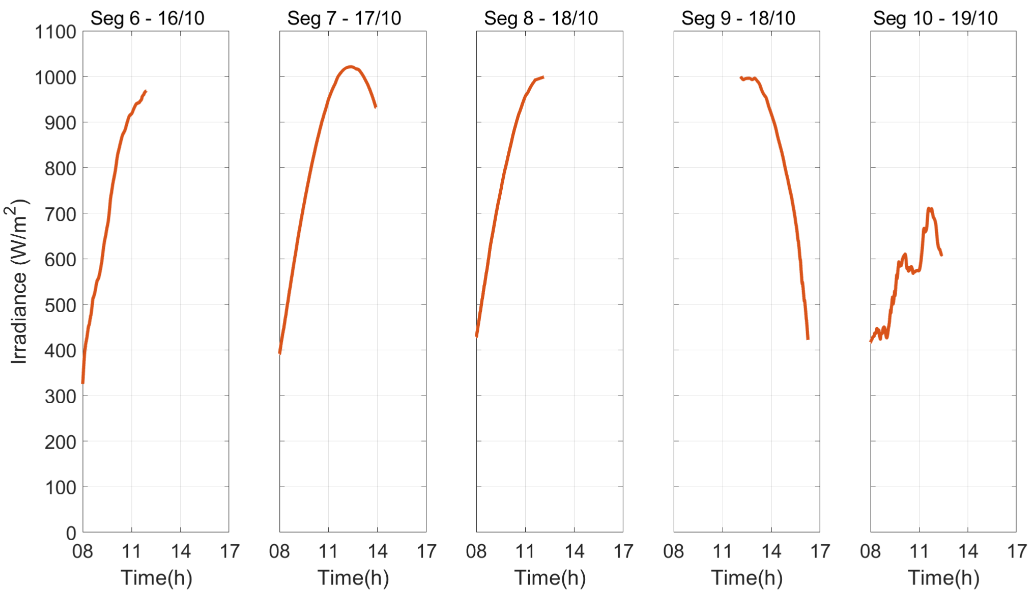

Figure 4.8: Irradiance throughout the 6^{th} and 10^{th} segments.

4.3.3 Wind Speed

Figures (4.9) and (4.10) show the behavior of wind speed and direction observed during each segment of the competition. It is important to recall that only the wind component in the same direction as the vehicle's movement is considered in this analysis. The positive wind speed values indicate that the wind is blowing from the rear of the vehicle, providing assistance in movement. Conversely, negative values indicate the opposite. In order to facilitate wind speed analysis, the Table (4.3) contains the wind speed medians, minimum and maximum values for each segment.

It can be observed that when the vehicle traverses segments 1, 2, 5, 6, 7, 8, and 10, the wind direction changes at least once. In contrast, during segments 3, 4, and 9, the wind direction remains constant, maintaining negative values. As the aerodynamic drag force constitutes one of the components of the total traction force, the vehicle is subjected to considerable additional resistance from this component during these three segments.

It can be observed in the fifth row of the Table (4.3) that the segments with the least pronounced fluctuations between the maximum and minimum values are the first, the third, the fifth, and ninth, with a difference of less than 2 m/s. As previously mentioned, the vehicle traverses a more desert-like region of the competition route from the fourth to the ninth segment. In these segments, with the exception of the fifth and the eighth, the absolute values of the median wind speed are among the highest, which is an important factor to consider. Outside this desert zone, the highest medians are those of the third and tenth segments, which mark the transition from this zone to a greener environment. The first two segments have the lowest medians, which coincides with the greener areas of the competition.

Table 4.3: Wind speed minimum, median and maximum values during each segment of the World Solar Challenge.

Segment	Min [m/s]	Median [m/s]	Max [m/s]	Difference [m/s]
1	-0.53	**0.03**	0.91	1.44
2	-0.52	**0.34**	1.76	2.28
3	-1.68	**-1.04**	-0.38	1.30
4	-2.75	**-1.58**	-0.03	2.73
5	-1.29	**-0.44**	0.43	1.73
6	0.35	**2.09**	3.35	3.00
7	-1.00	**1.36**	2.16	3.16
8	-0.92	**0.41**	1.30	2.22
9	-2.15	**-1.39**	-0.40	1.75
10	-1.11	**0.94**	1.72	2.84

Figure 4.9: Wind speed throughout the 1st and 5th segments.

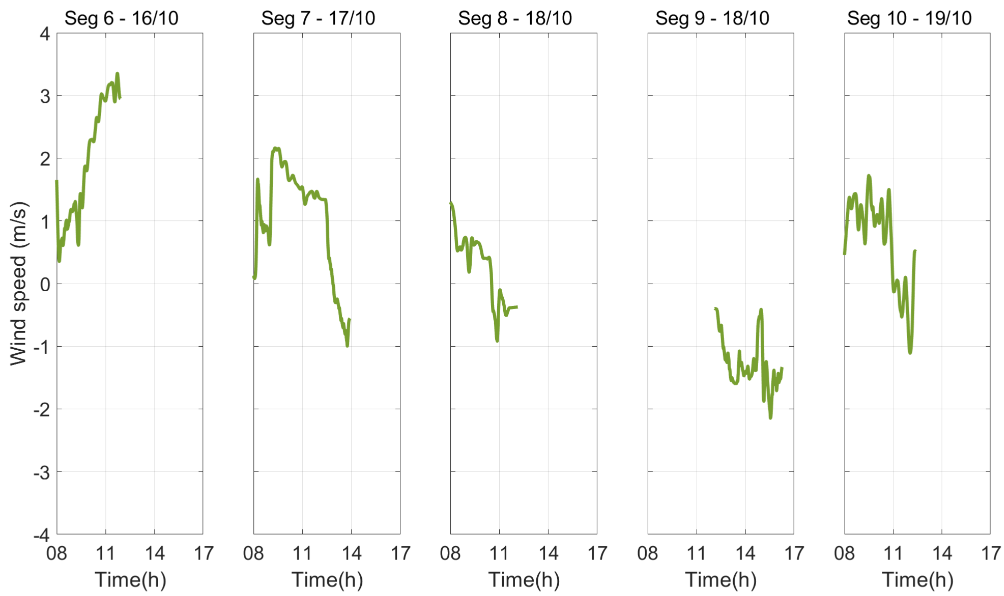

Figure 4.10: Wind speed throughout the 6th and 10th segments.

4.3.4 Altitude

After obtaining the altitude variations along the competition segments, the numerical model utilizes the following approximations, as illustrated in Figures 4.11 and 4.12, achieving a similar behavior as in [34]. In the first five segments, there is an upward tendency in altitude along the routes. However, from the sixth segment to the ninth, a progressive decrease in altitude is observed. The tenth segment of the route culminates at a higher altitude than the initial point. Furthermore, more accentuated fluctuations in altitude are discernible in select segments, exemplified by the initial phase of the seventh segment. Additionally, fluctuations in altitude values are evident in various segments, including the fourth and eighth.

It can be reasonably assumed that the variation in altitude directly affects the component of the vehicle's gravitational force that will act on the vehicle. One may reasonably infer that during both the first five and tenth segments, an increase in gravitational force is necessary to enable the vehicle to traverse those segments at the desired speed, given the corresponding increase in altitude. Conversely, during the segments in which altitude decreases (segments six to nine), the gravitational force will act to facilitate the vehicle's movement, thereby requiring less power from the vehicle.

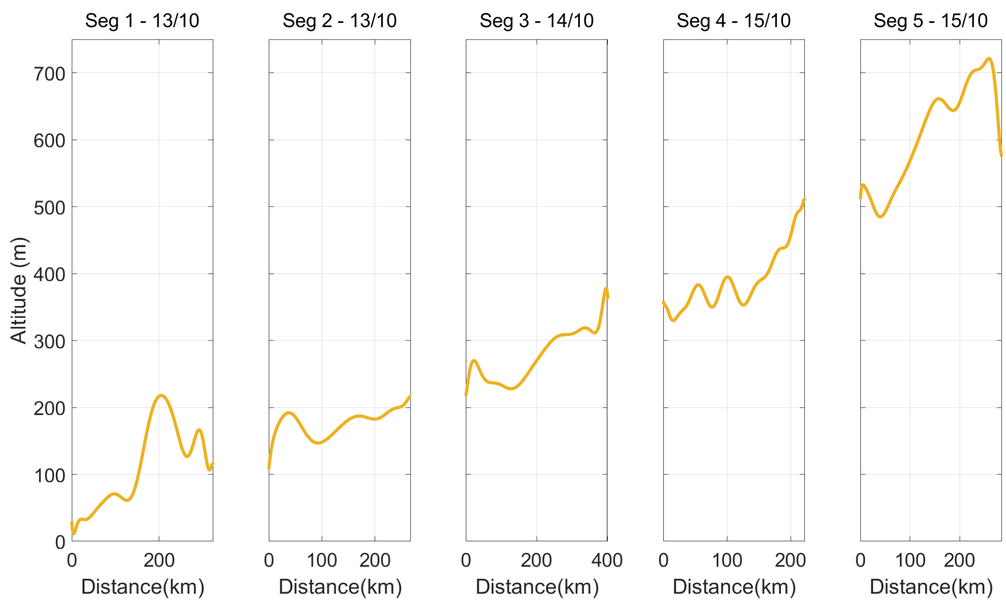

Figure 4.11: Altitude throughout the 1st and 5th segments.

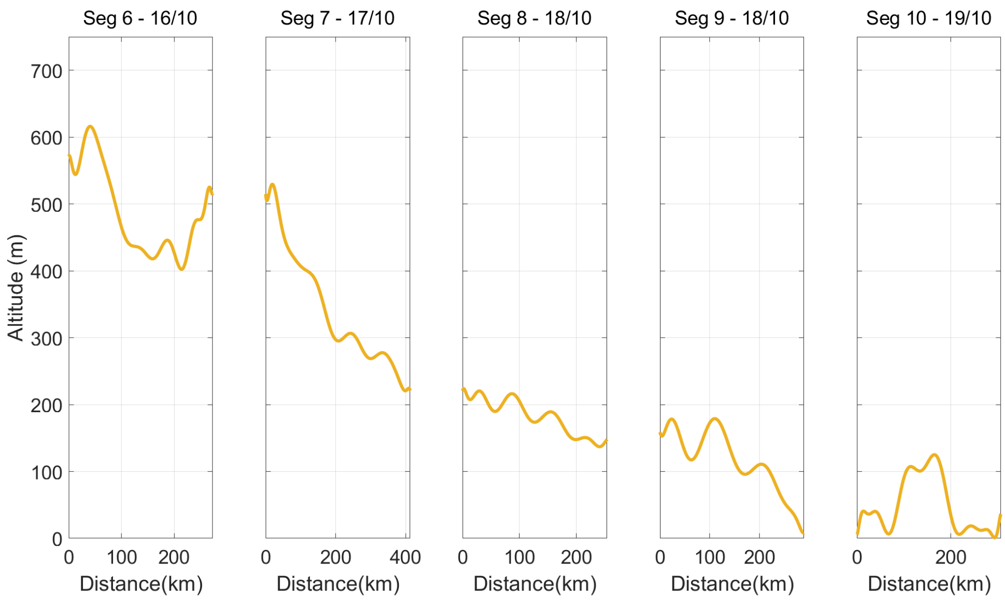

Figure 4.12: Altitude throughout the 6th and 10th segments.

4.4 Results of the First and Second Segments of the World Solar Challenge

This section presents the results of the model in which a vehicle traverses segments of the World Solar Challenge at a speed of 70 km/h. For the results below, it is decided to perform them with an area of photovoltaic panels equivalent to 1.58 m^2, representing a peak power of 354 W under standard test conditions, that is, for an irradiance of 1000 W/m^2 and a cell temperature of 25 ℃, while keeping the remaining parameters chosen for the vehicle. This analysis allows for a more detailed examination of the input and output power, temperature, and efficiency of the photovoltaic panels, the vehicle's consumption throughout the segments, and a comparison of the energy produced by the panels and the energy consumed by the vehicle.

Figure (4.13) illustrates the behavior of the input and output powers of the photovoltaic panels (warm colors), along with their temperature (in green) over time, for the first two segments. The first dashed vertical line represents the end of segment 1, and the second dashed line marks the start of the second segment. It can be observed that during the first segment, there is an increase in the input and output powers of the photovoltaic panels, as well as a simultaneous increase in their temperature. While the vehicle is stationary, between the end of the first segment and the beginning of the second, both power and temperature remain relatively constant. From the second segment onwards, there is a decrease in the panels' input and output powers, while the temperature begins to decline at approximately 14:00h.

As shown in [35], the panel's temperature reaches values much higher compared to the maximum of 40 ℃ for the ambient temperature, with an average cell temperature of 60 ℃.

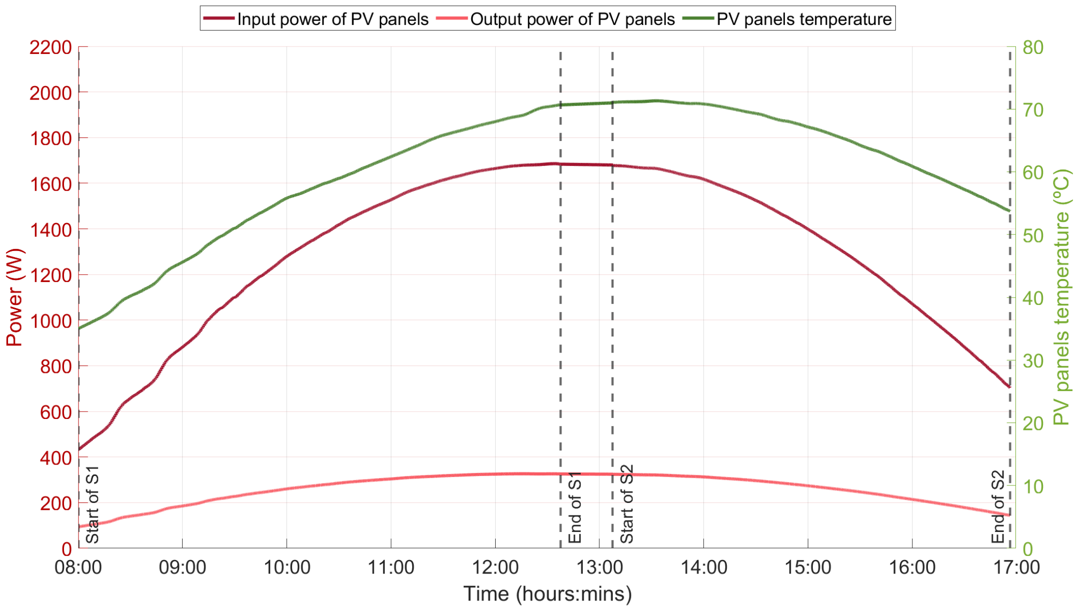

Figure 4.13: Photovoltaic panels input and output power and temperature during the 1st and 2nd segments of the World Solar Challenge.

Observing the efficiency behavior in Figure (4.14) with the assistance of Figure (4.13), one may notice three distinct zones throughout both segments for the efficiency. The first zone (red) is characterized by the most significant reduction in efficiency, which can be attributed to, the fact that the temperature of the panels rises from 35 ℃ (the initial value) to 71 ℃, that is, two times its initial value. This has a negative impact on the output power, consequently affecting the efficiency. This is confirmed by the significant increase in the input power, which exceeds the increase in the output power of the panels. As the input power increases from 433 W to 1683 W, representing a rise of 3.9 times its initial value, the output power rises from 94 W to 326 W (3.5 times). Given that efficiency is defined as the quotient between the output and input powers, a decrease in efficiency is to be expected, given that the output power increases more in percentage. This results in an efficiency decrease of 2.4%, from 21.7% (maximum efficiency during both segments) to 19.3%.

The second zone (yellow) occurs between the end of the first segment and 14:00h. This period shows an almost constant efficiency, due to the constant values of the photovoltaic panels. During this interval, the efficiency values are the lowest due to the high temperatures of the photovoltaic panels, reaching a minimum of 19.3%.

The third zone (green) of the efficiency curve demonstrates an increase in efficiency due to a reduction in panel temperature from 70.8 ℃ to 53.7 ℃, representing a 17 ℃ (24%) decrease from the initial value of this zone. To verify the efficiency behavior, it is sufficient to apply the same reasoning used in the first zone. This line of reasoning suggests that an increase in the ratio of output power to input power will result in an equivalent increase in the efficiency of the panels. The output power decreased by 169 W (from 313 W to 144 W), representing a 54% reduction relative to the initial value observed in the green zone. The input power also declined, dropping from 1617 W to 703 W, representing a 57% reduction. Given that the decline in the input power surpassed that observed in the output power, it can be confirmed that the efficiency increased. It is expected that during each day of the competition, the panels' efficiency curve will present a similar behavior. During this segment, the difference between the maximum and minimum values is 2.4%. Furthermore, it has been observed that the panels demonstrate higher output power values when their efficiency is lower throughout the entire day.

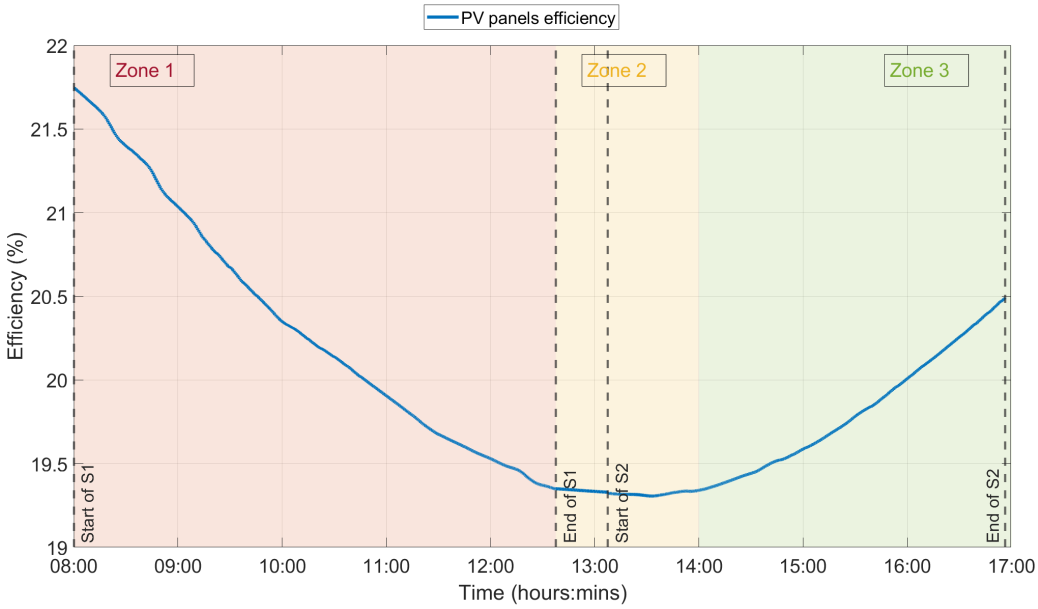

Figure 4.14: Photovoltaic panels efficiency during the 1st and 2nd segments of the World Solar Challenge.

In Figure (4.15), one observes the traction power, P_t, and its components required for the vehicle to move along the first and second segments of the World Solar Challenge. Here, P_d represents aerodynamic drag power, P_g' denotes the gravitational power component, P_{roll} stands for the frictional power between the ground and the wheel, P_t is the power required by the wheel for the vehicle to move at the desired speed of 70 km/h, traction power. The power values of P_t and its components shown are those required at the wheels, as illustrated in Figure (3.5). When the traction power shows negative values, it means that the power flow is directed from the photovoltaic panels and/or the battery pack to the motor. The remaining power components follow the same logic, as they are components of the traction power, helping to understand which component has more impact during the segments..

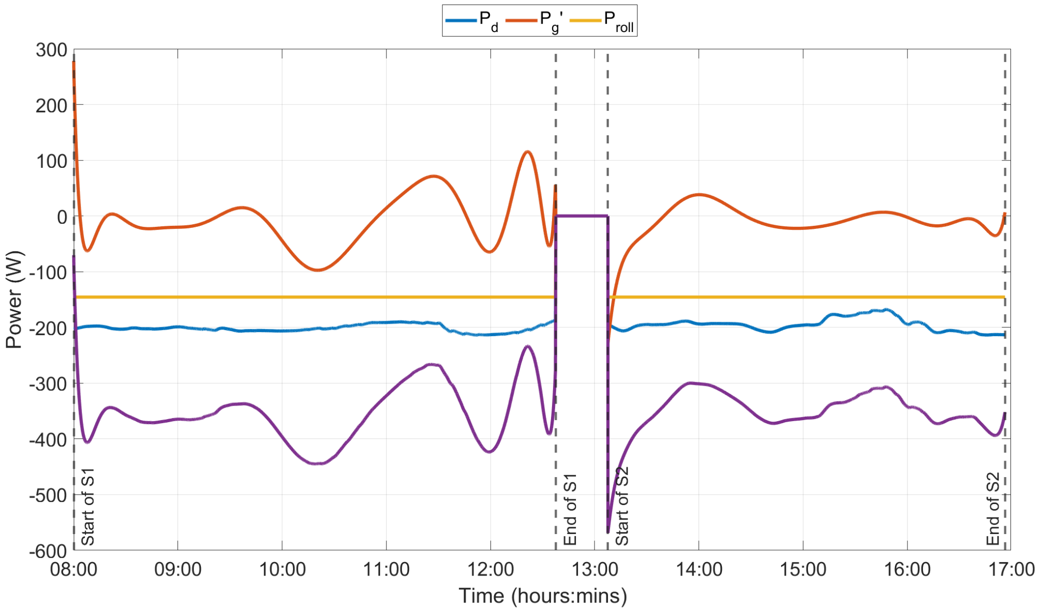

Figure 4.15: Traction power required at the wheel and its components for the 1st and 2nd segments of the World Solar Challenge.

Figure (4.16) depicts the relationship between aerodynamic drag power, P_d, and wind speed as a function of time during the second segment of the World Solar Challenge. When the wind speed is negative, the wind blows from the front of the vehicle, impeding its forward motion. Conversely, when the wind speed is positive, the wind provides assistance to the vehicle's movement, blowing from its rear. With regard to P_d, the flow of power is consistent with the previous paragraph, whereby when the power is negative, the flow of power is directed from the battery pack/panels to the motor. It is evident that the wind speed values exhibit considerable fluctuations during the second segment, exerting a pronounced influence on P_d. During this segment, the maximum absolute value is 214 W, and the minimum is 168 W, representing a difference of 46 W. This difference accounts for 21% of the maximum aerodynamic drag power value throughout this segment.

Upon comparison of the magnitude of P_d with that of the other components of traction power, P_t, as illustrated in Figure (4.15), it can be observed that this component possesses the largest absolute value during the first two segments, thereby contributing the most to the vehicle's consumption. A comparison of the 46 W mentioned above with the traction power along the two segments reveals that this fluctuation is not as significant as it may initially appear. When considered in relation to the maximum value of P_t, which is 569 W, this represents 8% of it. However, when compared with its average value along the route of 352 W, it represents a significant variation of 13% of the vehicle's total consumption to maintain a speed of 70 km/h.

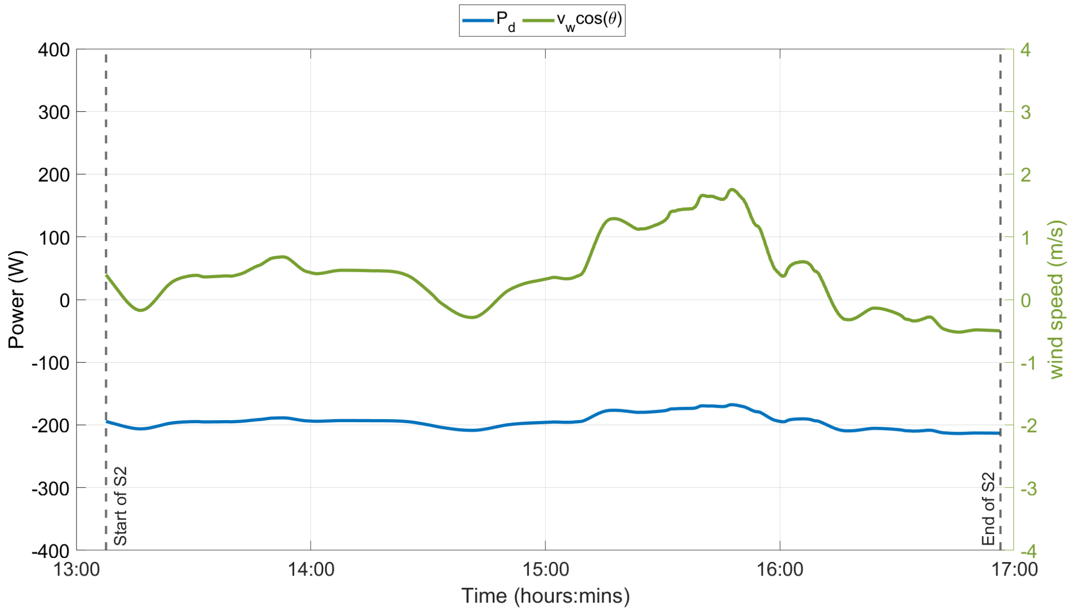

Figure 4.16: Aerodynamic drag power and wind speed of the second segments of the World Solar Challenge.

In relation to the gravitational power component, P_g', the fluctuations observed in Figure (4.15) throughout the first and second segments indicate significant altitude changes during both segments. However, it is noted that P_g' contributes the least to the increase in power required for the vehicle's movement. This is substantiated by the median values of P_g' during the first and second segments, which are -13 W and -10 W, respectively.

The rolling friction power,P_{roll}, remains constant across the segments, since the route is always in a highway. This power represents the component of P_t with the second highest impact during the competition.

Regarding to the power component P_t illustrated in Figure (4.15), it is evident that this power exhibits considerable fluctuations across the various segments. This phenomenon can be attributed to variations in P_g', which is a direct consequence of the altitude changes experienced along the route. During the mandatory stop, all powers are observed to be equal to zero, reflecting the vehicle's stationary state.

It can also be observed that despite the considerable fluctuations in P_g', it is the power that contributes the least to the increase in vehicle consumption along the route. In some instances, this power helps to move the vehicle, while in others it serves to reduce consumption on downhill sections. In contrast, the component that contributes the most to the increase in vehicle consumption is P_d, although this may change if the vehicle weight changes due to a alteration such as increasing the photovoltaic area.

Figure (4.17) illustrates the power consumed by the vehicle, which represents the negative part of P_t at the output of the charge controller, and the power produced by the panels, also at the output of the charge controller, during the segments 1 and 2 of the competition. With regard to the power consumption, there are several variations due to the gravitational and aerodynamic drag power components, as previously explained. Furthermore, the power values required to move the vehicle have increased in comparison to Figure (4.15), due to the consideration of the efficiencies of the DC/DC converter, the DC machine, and the gearbox, which together result in a combined efficiency of 54.2%. In comparison to the data presented in Figure (4.13), the power generated by the solar panels exhibits a reduction. This is attributed to the consideration of the charge controller's 85% efficiency. It can be observed that the panels are unable to generate the full amount of power necessary for the vehicle to move. It is notable that the interval during which the power consumed is 0 W coincides with the vehicle being stationary. Conversely, when the vehicle is in motion, the panels are unable to supply the requisite power. Nevertheless, there is a notable reduction in the power supplied by the battery pack, given that the average power consumption during the two segments is approximately 652 W, while the average power produced by the panels is approximately 218 W, representing approximately 33% of the consumption.

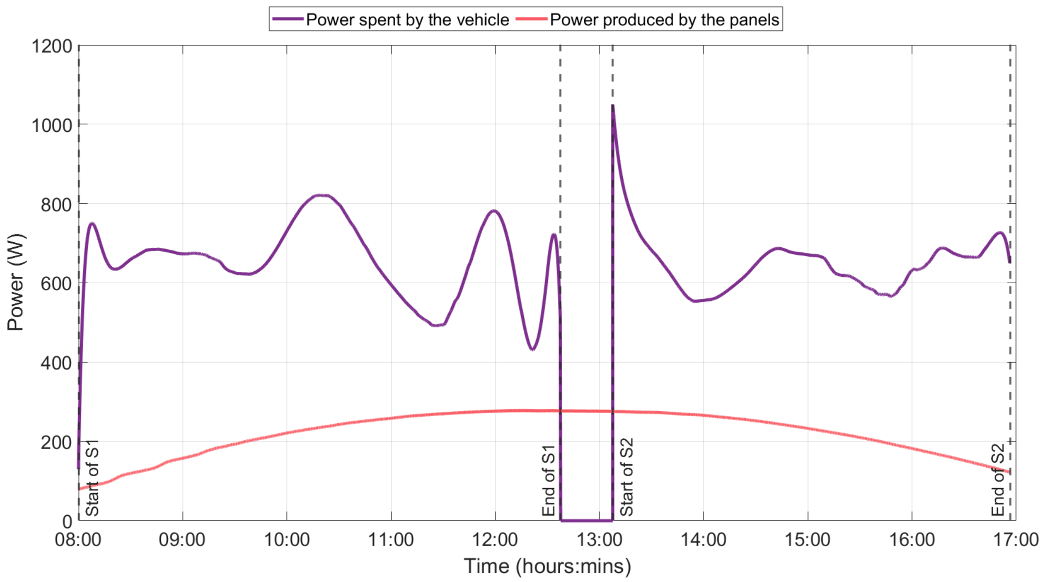

Figure 4.17: Produced and consumed powers for the 1st and 2nd segments of the World Solar Challenge.

The state of charge (SOC) of the vehicle's battery pack, the charge and discharge of the battery during the first two segments, is shown in Figure (4.18). The blue curve represents the state of charge of the battery pack, with the photovoltaic panels producing energy, while the orange curve shows how the battery would discharge during the first and second segments in the absence of the input power provided by the photovoltaic panels. In order to clarify the percentage pf energy increase in the battery, it is necessary to analyze the two curves. It should be noted that the state of charge of the battery pack cannot be less than 10%, in order to guarantee the vehicle's overall functionality. In the absence of photovoltaic panels, the vehicle would need to stop moving at approximately 14 hours. While with the panels, it reaches this same limit at approximately 17 hours, since at 14 hours, the battery pack has 33% more capacity, allowing it to maintain a speed of 70 km/h for an additional three hours, enabling it to complete the remaining 192 km of the second segment, which would be impossible without the photovoltaic panels. At the end of this day, the photovoltaic panels produced 28.6% of the energy spent by the vehicle.

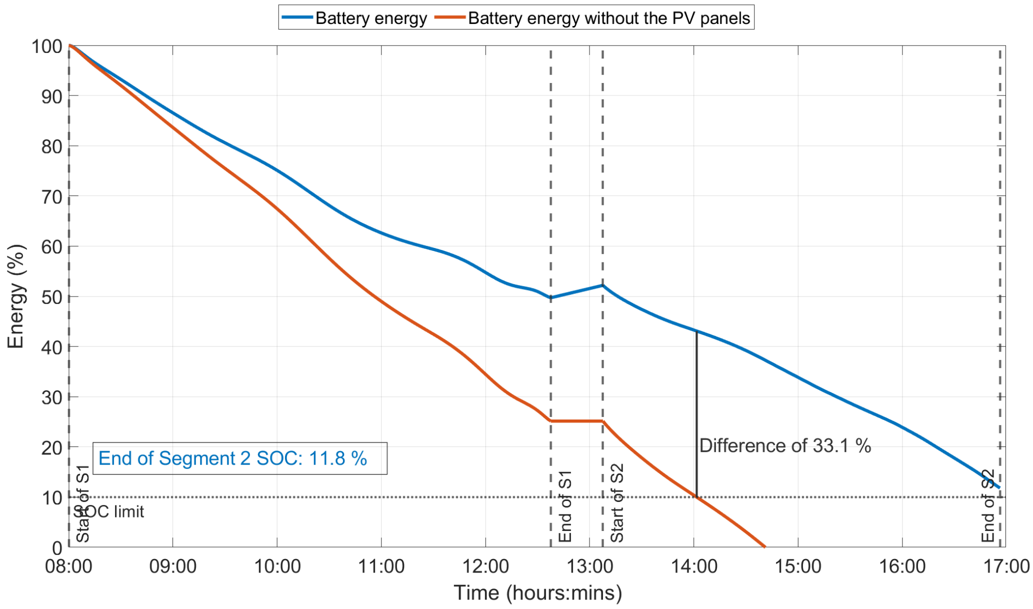

Figure 4.18: State of Charge when the vehicle travels at a speed of 70 km/h for the 1st and 2nd segments of the World Solar Challenge.

Figure (4.19) provides an illustration of the vehicle's position and the state of charge of the battery pack for each 30-minute interval, along with the starting and stopping times and the total distance traveled for the first two segments of the competition. Additionally, it indicates the increase in the state of charge of the battery pack during the 30-minute mandatory break between both segments, charging 2.5% of the battery pack. Figure (4.20) maps the competition route, with the completed segments highlighted in orange, covering a total distance of 591 km. In white are the segments to complete.

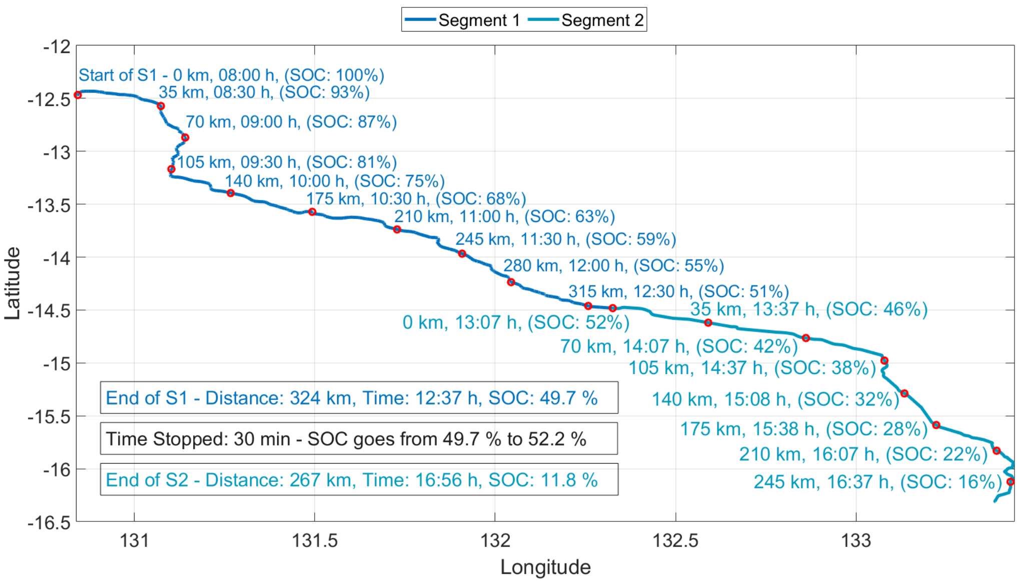

Figure 4.19: World Solar Challenge 1st and 2nd segments route.

Figure 4.20: World Solar Challenge completed segments 1 and 2.

4.5 World Solar Challenge Results

This section presents the numerical model results for the remaining segments, with a view to determining whether the planned strategy of completing the competition at a speed of 70 km/h in all segments can be achieved. This depends on the final energy at the end of each segment. The analysis identifies the segments with the greatest difficulty, taking into account the specific conditions presented in each segment, the battery capacity at the end of each segment, and the energy produced by the photovoltaic panels relative to the vehicle's total consumption.

Figure (4.21) illustrates the total energy required at the charge controller output, comprising the following components: wheel friction with the ground (yellow), aerodynamic drag (blue), and gravitational (orange). The sum of these components is equal to the total energy required at the charge controller output. It is noteworthy that the aerodynamic drag consistently represents the most significant component in all competition segments, reinforcing the necessity to minimize the resistance associated with this component. The component representing wheel friction remains the second-largest throughout all segments, with similar magnitude compared to the aerodynamic component, thereby indicating that it is of equal importance to reduce the friction between the vehicle's wheels and the ground, as well as to maintain a minimum vehicle weight, which is a priority in [36] and [37]. The gravitational component is significantly smaller in comparison to the other components, which is a consequence of the vehicle's lightweight construction and a total mass of 142.5 kg (including the driver). With regard to the segments with the highest energy consumption, it is evident that the third and seventh segments require the most energy, which is an expected outcome given that they are the longest segments of the competition.

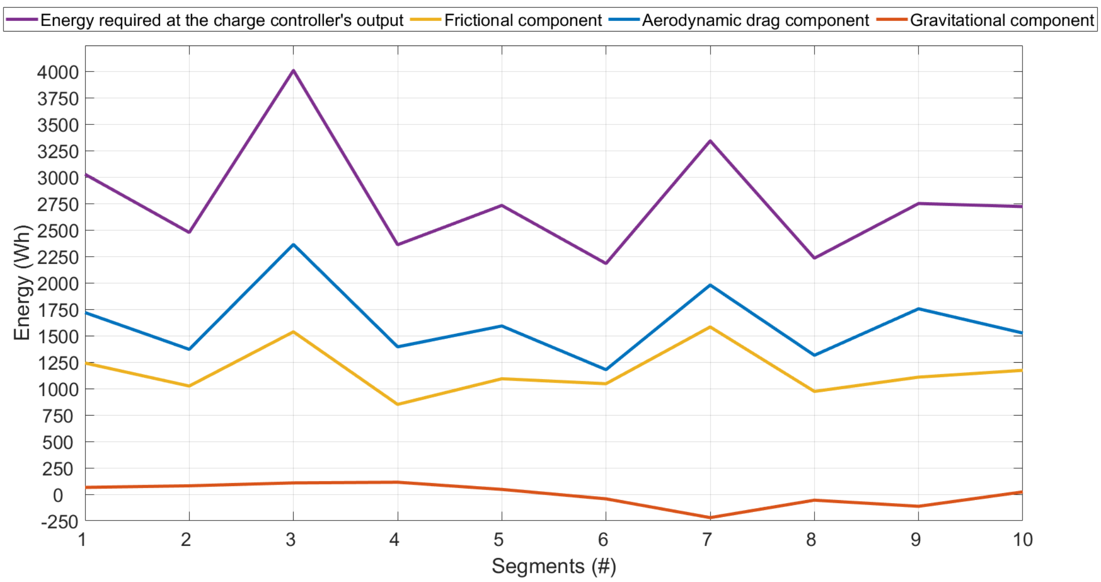

Figure 4.21: Energy required at the charge controller output, with frictional, aerodynamic, and gravitational components for each segment of the World Solar Challenge.

It is notable that, despite the total distance of the third segment being 401 km and that of the seventh segment being 413 km, the third segment requires approximately 700 Wh more at the charge controller output, being around 17% more. This discrepancy can be attributed to the differing energy requirements for the gravitational and aerodynamic components in each segment. A comparable discrepancy is observed when comparing segments four and six, in which the fourth segment exhibits a higher consumption despite its shorter length. Projecting forward to future competitions, it is expected that the segments with the highest energy consumption will be the first, third, fifth, seventh, ninth, and tenth, particularly if the competition occurs on dates similar to those utilized, from October 13 to 20. Overall, the aerodynamic component accounts for more than 50% of the vehicle's consumption during the competition, and the friction component accounts for around 40%.

It is confirmed that, with the considerations made, it is possible for the vehicle to complete all segments of the competition according to the planned schedule, obtaining the values presented in Table (4.4). This table indicates the state of charge (SOC) of the vehicle's battery pack at the beginning and end of each segment, as well as the battery discharge. It also shows the distance traveled and the time required to complete each day of the competition, taking into account the mandatory break time between segments. It is important to note that each day of the competition has a time limit of 9 hours.

It can be observed that on the first day, it is possible to complete two segments. However, the vehicle finishes the second segment with the battery very close to the proposed limit of 10% of its maximum capacity. Furthermore, it is observed that the vehicle completes the second segment with four minutes remaining before the deadline for arrival on the 13th day. This highlights the importance of considering an increase in the vehicle's speed on some stretches of the first two segments. Given that the battery capacity at the end of this day is already very close to the defined limit, it may be beneficial to consider increasing the battery capacity and/or expanding the photovoltaic area on the vehicle. However, it should be noted that these changes will increase the vehicle's weight, and it is, therefore, necessary to assess how beneficial they would be in reducing the time required to traverse the segments, as well as for the state of charge (SOC) at the end of each segment. On the 15th day, the vehicle completes the fifth segment with a state of charge (SOC) below 15%, which is also close to the battery limit. In the remaining days, the vehicle's battery shows a state of charge (SOC) above 20%. In such instances, it may be advantageous to consider increasing the vehicle's speed in order to complete certain segments faster, thereby reducing the overall time required to complete the competition. As with the preceding analysis of the difficulty of each segment, it is observed that at the conclusion of the first, third, seventh, and tenth segments, the battery exhibits a pronounced discharge, reaching values near or exceeding 50% of its total capacity, thereby demonstrating the considerable challenge posed by these segments. Overall, a reduction in battery state of charge of 1% during the competition is equivalent to an average distance of 6.5 km travelled by the vehicle. The results show that, with the considerations made, it is possible to complete the competition in 44 hours and 49 minutes.

Table 4.4: State of charge and discharge of the vehicle's battery, distance traveled at the end of each segment of the World Solar Challenge, and total time required for each day of the competition.

Day of October		13		14	15		16	17	18		19
Segment		1	2	3	4	5	6	7	8	9	10
Distance [km]		324	267	401	222	285	273	413	254	289	306
SOC [%]	Start	100	52.2	100	100	59.8	100	100	100	66.7	100
	End	49.7	11.8	34.0	57.4	14.4	65.8	52.0	64.3	22.3	50.5
Battery Discharge [%]		50.3	40.4	66.0	42.6	45.4	34.2	48.0	35.7	44.4	49.5
Time [hours:mins]		08:56		05:43	07:44		03:54	05:53	08:15		04:22

In Table (4.5), the percentage of consumed energy that was generated by the photovoltaic panels is presented. The average energy produced by them throughout all the days of the competition is around 28% of the consumed energy. It is notable that on day 17, a greater quantity of energy is produced than on the rest of the days of the competition. This occurrence can be attributed to the favorable environmental conditions previously analyzed, recalling that on this day, the ambient temperature does not exceed 25℃, and the irradiance values can exceed 1000 W/m^2. On day 19, despite the ambient temperature being below 17℃ and the irradiance reaching maximum values of 700 W/m^2, the photovoltaic panels achieved a production of 21% of the energy consumed throughout the tenth segment, which is a positive outcome, particularly given that it represents the lowest energy production during the entire competition. It can be reasonably assumed that in more adverse environmental conditions, the energy production from the panels will decrease by 7% in comparison to the vehicle's total consumption during a segment. This implies that in more challenging environmental conditions, the battery must provide an additional 7% of the vehicle's total consumption during a segment.

Table 4.5: Proportion of energy consumed that is generated by photovoltaic panels each day during the World Solar Challenge.

Day of October	13		14	15		16	17	18		19
Segment	1	2	3	4	5	6	7	8	9	10
Energy generated [%]	28.6		26.6	25.9		29.4	34.3	30.2		20.6

Since the aerodynamic drag power component is one of the major causes of the vehicle's energy consumption, in an effort to understand and reduce this consumption, Figure (4.22) demonstrates the variation of battery energy at the end of the first segment as a function of the aerodynamic coefficient, C_d. It can be observed that varying the aerodynamic coefficient leads to a linear change in the remaining energy of the battery pack when the vehicle reaches the end of the first segment. Specifically, a 0.01 increase in the aerodynamic coefficient results in a 4.2% decrease in the vehicle's battery pack energy at the end of the first segment. It is important to note that this variation is based on data from the day the vehicle travels the first segment (October 13, 2019).

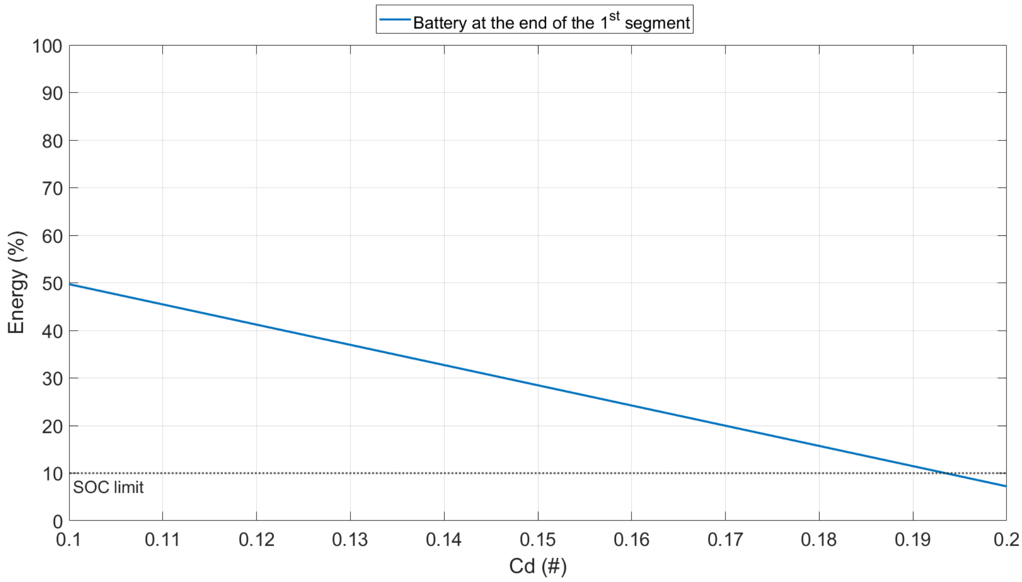

Figure 4.22: Variation of the battery energy at the end of the 1st segment in function of the aerodynamic coefficient, C_d.

The Table (4.6) illustrates the variations in energy at the end of each segment of the World Solar Challenge, with a 0.01 increase in the aerodynamic coefficient. The data indicates that during the days of the competition, the second, fifth, and ninth segments exhibit the most pronounced decline in battery energy as the aerodynamic coefficient increases. This observation suggests that these segments are the most susceptible to aerodynamic resistance caused by wind. This is due to the fact that these segments are traveled subsequent to the vehicle's having completed a preceding segment on the same day. Consequently, the battery's initial energy is influenced by the energy it possesses at the conclusion of the preceding segment, which in this case is segments 1, 4, and 8. Thus, using the second segment as example, the variation in the aerodynamic coefficient in the first segment affects its final battery value, thereby altering the initial energy of the second segment and influencing the energy with which the vehicle finishes the second segment. The sixth segment of the competition exhibits the least variation in battery energy as C_d increases, with a variation of -2.9%, indicating that the vehicle is comparatively less affected by aerodynamic resistance during this segment.

The variations in battery energy are approximately -3% or more for every 0.01 increase in C_d. Given that when two segments are traversed on the same day, the variation of the second segment is significantly more negative, it can be posited that running two segments a day is an ideal way of completing the competition as quickly as possible. Furthermore, reducing the vehicle's aerodynamic coefficient will result in a reduction in the energy required to overcome aerodynamic resistance, thereby increasing the possibility of crossing two segments in one day. It is acknowledged that this coefficient is already considerably low; however, this analysis substantiates the importance of maintaining the coefficient at a value that is as close as possible to the 0.1 used, as indicated in the article cited in reference to the competition [38], the average aerodynamic coefficient of the vehicles participating in the competition is a little above than 0.105. Given that the aerodynamic coefficient is already relatively low, there is potential for a reduction in the rolling resistance coefficient of 0.0051, thereby providing the opportunity for further improvements.

Table 4.6: Variation of the battery energy at the end of each segment of the World Solar Challenge, with an increase of 0.01 in the aerodynamic coefficient, C_d.

Segment	1	2	3	4	5	6	7	8	9	10
Energy Variation [%]	-4.2	-7.6	-5.8	-3.4	-7.4	-2.9	-4.9	-3.2	-7.6	-3.8

5

Conclusion

Contents

5.1 Project Conclusion

The principal objective of this thesis is to assist the team Mobile Energy Sustainability Project (Projeto Sustentabilidade Energética Móvel) (PSEM) to a future size of an electric vehicle to participate in the Bridgestone World Solar Challenge, with photovoltaic cells as the main energy source of the vehicle, .

A comparative analysis was conducted between the current competition and the other global solar competitions, identifying specific differences in track and vehicle characteristics, in order to select which competition the team would participate in, the PSEM team demonstrated a greater enthusiasm for focusing the study on the World Solar Challenge competition, which subsequently became the primary focus of the analysis.. The ILumen European Solar Challenge, in Belgium, demonstrates the highest photovoltaic efficiency; however, the World Solar Challenge was selected due to its international prestige, showing also the second-highest photovoltaic power output among the competitions studied. The environmental data for the 2019 World Solar Challenge event, during which the vehicle travels the ten segments at a speed of 70 km/h, is obtained. Based on the provided data, the forces acting on the vehicle throughout the competition were incorporated into the developed model, which calculates the battery's state of charge at the conclusion of each segment, the time required to complete the segment, and, in the case of completing consecutive segments on the same day, it indicates the starting time and battery state of charge at the beginning of that segment. The results demonstrated that when two segments are completed on the same day, the battery's state of charge at the conclusion of the final segment is significantly depleted, in some cases reaching a discharge of nearly 90% of its maximum capacity. The most significant energy consumption is attributed to aerodynamic resistance and friction between the vehicle's wheel and the ground. The photovoltaic array was capable of supplying approximately 28% of the energy required by the vehicle throughout the competition, with the worst-case scenario compensating for 21% of the energy consumption. Given the considerable energy consumption associated with aerodynamic resistance, the aerodynamic coefficient is identified as a fundamental parameter influencing the vehicle's performance. It is observed that for each incremental increase of 0.01 in this coefficient, the energy demanded from the battery increases by a minimum of 3% across the different segments of the competition.

It can be concluded that comparative analyses of the different competitions were successfully carried out, which were then followed by an analysis of its environmental conditions. A numerical model was initiated, as a tool to simulate the competitions, facilitating the acquisition of essential parameters for the vehicle's future sizing. This was achieved by using the collected environmental conditions as inputs, thereby demonstrating the energy required by the vehicle and the time necessary to successfully complete the World Solar Challenge. A small aerodynamic coefficient is essential for optimizing the vehicle's energy consumption. There is potential for improvement in the project, including the incorporation of acceleration and deceleration across the segments, as well as the impact of centripetal force on the vehicle's consumption, incorporating variable efficiencies for the motor and the battery, allowing to improve the numerical model and obtaining better simulation results. It is also important to assess the benefits of increasing the photovoltaic cell area and the feasibility of utilizing a higher-capacity battery, given that these alterations affect the vehicle's overall weight. Furthermore, an analysis of battery degradation based on its usage throughout the competition is a crucial aspect to consider for the vehicle's performance and the possibility of reducing the rolling resistance coefficient.

Bibliography

[1] Results, iet formula 24+, f24+ championship table. [Online]. Available: https://www.greenpower.co.uk/results

[2] Zero emission vehicles: first 'fit for 55' deal will end the sale of new co2 emitting cars in europe by 2035. [Online]. Available: https://ec.europa.eu/commission/presscorner/detail/%20en/ip_22_6462

[3] Mobile energy sustainability project (psem), gp23. [Online]. Available: https://psemportugal.com/garage/showroom?car=GP23

[4] Renishaw plc, greenpower. [Online]. Available: https://www.renishaw.com/en/greenpower--34626

[5] Coalescence car, hades. [Online]. Available: https://www.coalescencegp.co.uk/cars/hades

[6] S. Tamura, "Teijin's advanced carbon fiber technology used to build a car for the world solar challenge," *Reinforced Plastics*, vol. 60, no. 3, pp. 160–163, 2016.

[7] Sov class results. [Online]. Available: https://www.americansolarchallenge.org/2022/results/asc.html#:~:text=Overall-,SOV%20Class,-1st%20Place%3A

[8] Challenger class results. [Online]. Available: https://worldsolarchallenge.org/the-event/history/honour_roll#:~:text=2023%20EVENT-,Challenger%20Class,-1st%20Innoptus%20Solar

[9] Innoptus solar team, infinite. [Online]. Available: https://www.solarteam.be/en/cars/infinite

[10] Solar team twente, red x. [Online]. Available: https://www.solarteam.nl/discover-our-cars#:~:text=and%20increasing%20effiency-,2023%20%E2%80%93%20RED%20X,-RED%20X%20is

[11] Brunel solar team, nuna 12. [Online]. Available: https://nuna12.brunelsolarteam.com

[12] ilumen european solar challenge 2022, race, result. [Online]. Available: https://getraceresults.com/Results/organisator/2022/evenement/Zolder?race=iLumen+European+Solar+Challenge+2022

[13] Italian solar challenge 2022 race results. [Online]. Available: https://www.sonnenwagen.org/isc-2022

[14] Team sonnenwagen aachen, covestro adelie. [Online]. Available: https://www.sonnenwagen.org/covestro-adelie

[15] Solar challenge morocco 2021, results. [Online]. Available: https://classicevents.nl/solar-challenge-morocco-results/

[16] Winners of the 2022 sasol solar challenge. [Online]. Available: https://www.solarchallenge.org.za/content/solar-car-teams-awarded-their-achievement-2022-sasol-solar-challenge#:~:text=are%20as%20follows%3A-,Challenger%20Class,-Brunel%20Solar%20Team

[17] Solar competitions routes. [Online]. Available: https://www.google.com/maps/d/u/0/edit?mid=1yrE9uPGrDOqKrjxBgjzeAic4zpuS_sA&ll=4.788451340585475%2C-125.09905647103517&z=3

[18] Nrma control stops. [Online]. Available: https://worldsolarchallenge.org/files/2750_2023_bwsc_event_route_poster.pdf

[19] The final route version for the 2021 solar challenge morocco. [Online]. Available: https://classicevents.nl/solar-challenge-downloads/

[20] American solar challenge route. [Online]. Available: https://www.google.com/maps/d/u/0/viewer?mid=14uZZPPhrtfoTxX6XPClpYN0s3YFIlv_D&ll=43.969512136532174%2C-91.58443328344217&z=4

[21] Italian solar challenge, where. [Online]. Available: https://www.motoeng.co.uk/isc

[22] F1 track of circuit zolder in belgium. [Online]. Available: https://www.europeansolarchallenge.eu/#:~:text=F1%20track%20of%C2%A0Circuit%20Zolder%20in%20Belgium

[23] Carrera solar atacama 2018. [Online]. Available: https://scientificgems.wordpress.com/solar-racing/carrera-solar-atacama-2018/

[24] Sasol solar challenge route 2022. [Online]. Available: https://scientificgems.wordpress.com/2022/07/24/sasol-solar-challenge-2022/

[25] Pvgis website. [Online]. Available: https://re.jrc.ec.europa.eu/pvg_tools/en/

[26] Monocrystalline solar cel. [Online]. Available: https://pt.grandado.com/products/10-40-50-100-pces-2-8-w-125x125mm-barato-mono-celulas-solares-5x5-grau-a-monocristalino-fotovoltaico-pv-c gad_source=1&variant=UHJvZHVjdFZhcmlhbnQ6MjA0OTk3NDMz

[27] P. Fajri, R. Ahmadi, and M. Ferdowsi, "Equivalent vehicle rotational inertia used for electric vehicle test bench dynamic studies," in *IECON 2012 - 38th Annual Conference on IEEE Industrial Electronics Society*, 2012, pp. 4115–4120.

[28] Psem website. [Online]. Available: https://psemportugal.com/garage/showroom?car=GP23

[29] 2021 solar challenge morocco route segments. [Online]. Available: https://www.google.nl/maps/@30.9851143,-7.5793223,8z/data=!3m1!4b1!4m2!6m1!1s1fsV9tvaBaN5n9cvvOA-2vRdfmwKuauXr

[30] World solar challenge route segments. [Online]. Available: https://www.google.com/maps/d/u/0/edit?mid=1AhW65gVk3agFkSwLa7eJdQTJQPPCtCc&usp=sharing

[31] Weather query builder. [Online]. Available: https://www.visualcrossing.com/weather/weather-data-services

[32] D. D. Smith, P. J. Cousins, A. Masad, S. Westerberg, M. Defensor, R. Ilaw, T. Dennis, R. Daquin, N. Bergstrom, A. Leygo *et al.*, "Sunpower's maxeon gen iii solar cell: High efficiency and energy yield," in *2013 IEEE 39th Photovoltaic Specialists Conference (PVSC)*. IEEE, 2013, pp. 0908–0913.

[33] Competitions primary study points. [Online]. Available: https://www.google.com/maps/d/u/0/edit?mid=1_D2jSea5jzUrEurivJ1SpWk2uTMLYCA&usp=sharing

[34] E. Yesil, A. O. Onol, A. Icke, and O. Atabay, "Strategy optimization of a solar car for a long-distance race using big bang — big crunch optimization," in *2013 IEEE 14th International Symposium on Computational Intelligence and Informatics (CINTI)*, 2013, pp. 521–526.

[35] A. Amelia, Y. Irwan, W. Leow, M. Irwanto, I. Safwati, and M. Zhafarina, "Investigation of the effect temperature on photovoltaic (pv) panel output performance," *Int. J. Adv. Sci. Eng. Inf. Technol*, vol. 6, no. 5, pp. 682–688, 2016.

[36] Z. Taha, R. Passarella, J. M. Sah, and N. B. Abd Rahim, "A review on energy management system of solar car," in *The 9th asia pacific industrial engineering & management systems conference*. Citeseer, 2008, pp. 3–5.

[37] K. Nogita, J. Kennedy, J. Amsler, M. Greaves, C. Tuesley, and T. Nishimura, "Lead-free solders for solar and electric vehicles - reflections on the bridgestone world solar challenge 2013 in "arrow1"," in *2014 International Conference on Electronics Packaging (ICEP)*, 2014, pp. 10–13.

[38] A. Truque Bertran, "Design of a vehicle for the world solar challenge," B.S. thesis, Universitat Politècnica de Catalunya, 2023.